A consistent approach to the definition of initial geometric imperfections for in-plane stability design of steel moment frames

Harry Slack, Fiona Walport [*], Hou Un Chan, M. Ahmer Wadee, Leroy Gardner

Department of Civil and Environmental Engineering, South Kensington Campus, Imperial College London, London SW7 2AZ, UK

ARTICLE INFO

ABSTRACT

Geometric imperfections can have a significant influence on the behaviour and ultimate resistance of steel structures. For the purposes of structural design, particularly design by geometrically and materially nonlinear analysis with imperfections (GMNIA), a suitable choice of imperfections, in terms of both amplitude and shape, is therefore required; an inappropriate choice of imperfections can lead to misleading results and unsafe resistance predictions. The development of a practical strategy for defining imperfection shapes in the in-plane GMNIA-based design of steel moment frames is the focus of the present study. The proposals are also suitable for GNIA-based design. Both overall sway imperfections (i.e. frame out-of-plumbness) and individual member bow imperfections, together with combinations thereof (i.e. sway-member imperfection combinations), are considered. Several methods for introducing imperfections are assessed. Each method is categorised depending upon whether the imperfection is established through: (1) direct definition or (2) the scaling of eigenmodes. The recommended direct definition-based method introduces a sway imperfection in sympathy with the applied lateral loading and member imperfections with alternating directions between storeys, as dictated by the column base boundary conditions. The recommended eigenmode-based method uses the first sway mode and determines the number of non-sway modes according to the eigenvalues under the design loading, with all non-sway modes for which the eigenvalues $\alpha_{cr,ns} < 25$ also contributing to the imperfection. The eigenmodes are scaled to ensure the bounds of the prescribed imperfection amplitudes are suitably maintained. The consistency and accuracy of the proposed methods are demonstrated for 21 different frame configurations.

1. Introduction

An appropriate allowance for geometric imperfections is a crucial part of structural stability design. The traditional approach to designing steel structures has been founded on a two-step process. The first step is to calculate the internal stress resultants within the structure under the design loading; this is normally accomplished through either a first or second order elastic analysis of the structure. The second step is to compare the internal stress resultants within each structural member with the corresponding design resistances, calculated according to semi-empirical design expressions provided by international standards. These calculations implicitly account for the effects of initial geometric imperfections and residual stresses. However, these design expressions can introduce simplifications or require assumptions that are not representative of the true structural behaviour, e.g. discontinuities introduced within cross-section classification [1] and idealisations made in determining member buckling lengths. Therefore, alternative design procedures have been proposed [2–8] that employ so-called advanced analysis, or geometrically and materially nonlinear analysis with imperfections (GMNIA), and circumvent the use of these design expressions; instead, the structural resistance is determined directly from within the finite element (FE) analysis. A key component of these GMNIA-based design methods is the explicit modelling of initial geometric and material imperfections. With increasing research attention, as well as growing use in practice, these methods have now been integrated into a number of international structural design standards [9–11]. While the results of design by GMNIA tend to be more accurate and consistent compared to the traditional two-step methodology, the structural models are necessarily more complex. In particular, the designer must consider carefully how the initial geometric imperfections are accounted for at the cross-section, member and system levels. The goal, as stated in current structural design standards, is to identify the most severe imperfection shape that leads to the lowest (i.e. safest) resistance for a given structure. Without sufficient guidance,

---
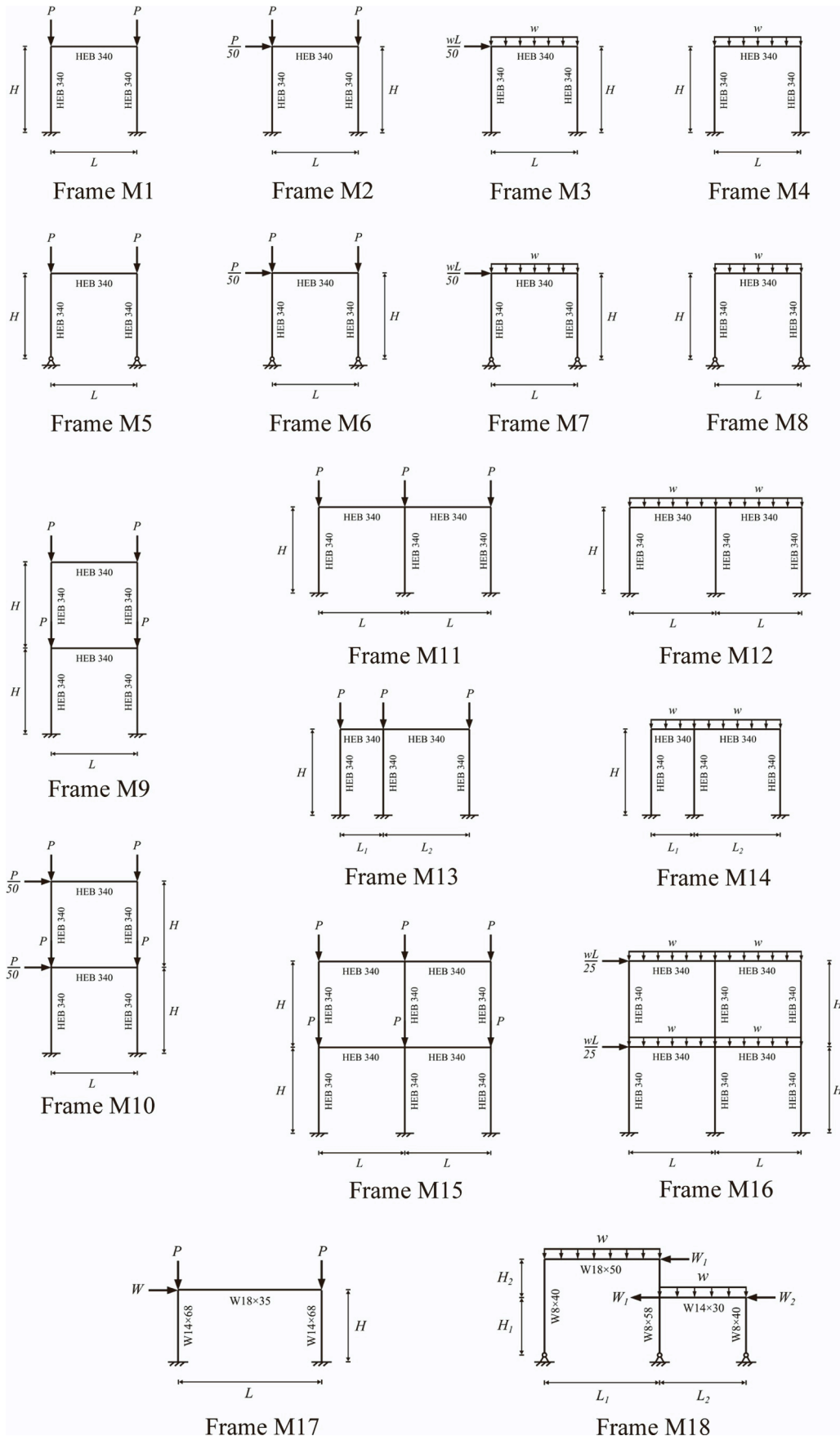
Fig. 1. Overview of the moment frame configurations considered herein.
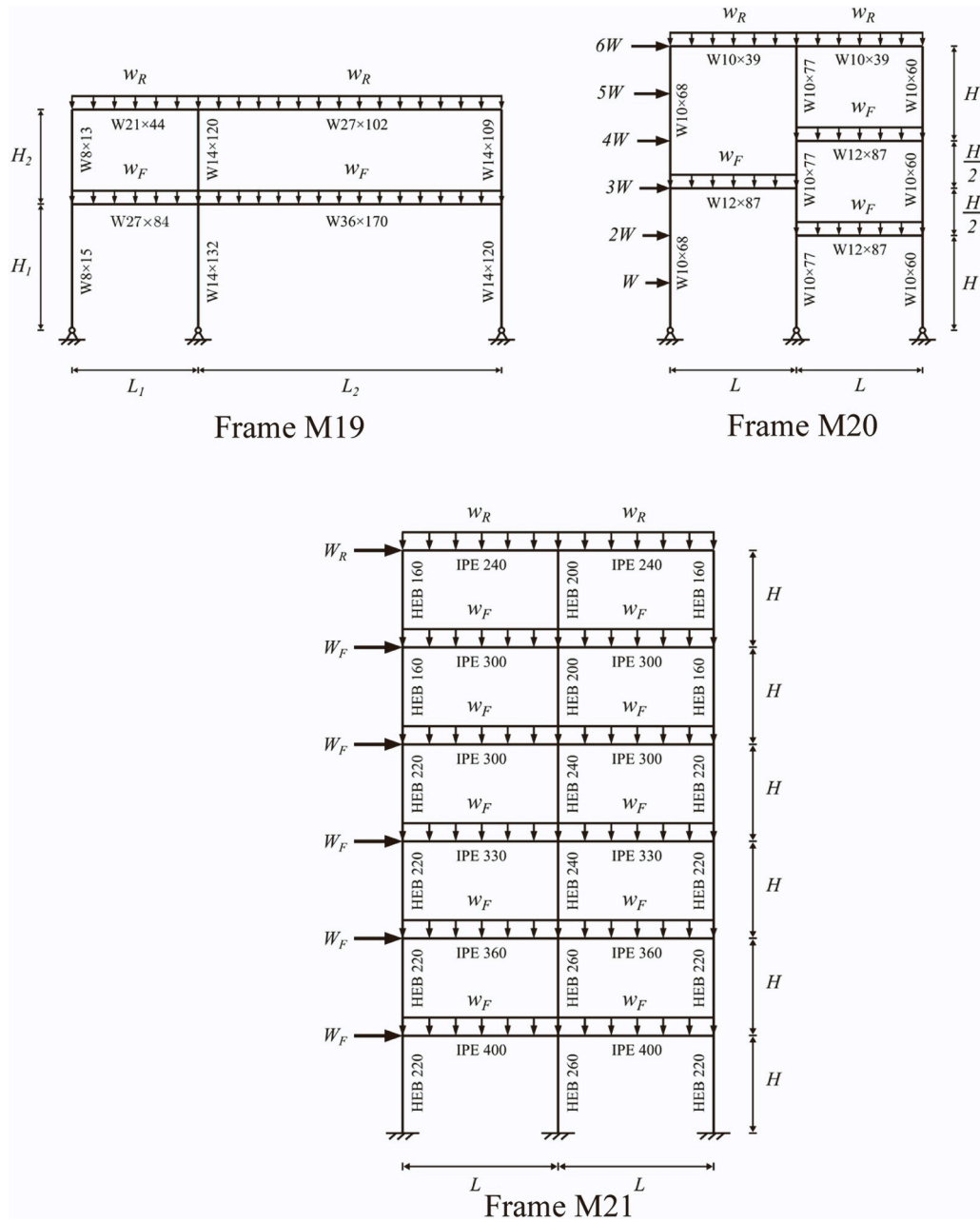
Frame M19

Frame M20

Frame M21

Fig. 1. (*continued*).

inconsistencies with regards to the adopted imperfections can occur and an inappropriate choice of imperfections can lead to misleading results and unsafe resistance predictions. Thus, there is a pressing need for a consistent and practical method to define geometric imperfections.

There are two key considerations when defining imperfections, namely the amplitude and the shape/direction of the imperfection. A number of recent studies have focused on deriving suitable amplitudes of imperfections, as well as strategies for combining them at the cross-section and member levels [12] and at the member and global frame levels [13]. For design by GMNIA or GNIA using beam finite elements, the influence of imperfections at the local cross-section level are accounted for through cross-section capacity or strain limit [1,7] checks. However, the direct modelling of global sway imperfections (i.e. frame out-of-plumbness) and individual bow imperfections, together with combinations thereof (i.e. sway-member imperfection combinations), are required and are thus considered herein.

There are four principal means of representing initial geometric

imperfections into finite element models: (1) directly modifying the nodal coordinates of the FE mesh; (2) superimposing scaled elastic buckling modes (eigenmodes) obtained from a linear buckling analysis (LBA); (3) imposing notional horizontal forces and (4) reducing the stiffness of each member. The first two are considered herein, with the primary focus of the present paper being to develop a method by means of which suitable imperfection shapes/directions can be introduced.

2. Benchmark frame modelling

Beam finite element models developed using the commercial package Abaqus [14] were used to determine the ultimate capacities of planar moment frames with varying initial imperfection shapes. Fig. 1 and Table 1 provide an overview of the 21 frame configurations modelled herein [15,16]. In this section, the general modelling approach and the validation of the beam FE models are presented.

Table 1
Dimensions and loads for frames considered herein, based on frames in [15,16].

Frame	Dimensions (m)	Loading
M1	$L = H = 10.0$	$P = 5880$ kN
M2	$L = H = 10.0$	$P = 4610$ kN
M3	$L = H = 10.0$	$P = 28.7$ kN, $w = 144$ kN/m
M4	$L = H = 10.0$	$w = 144$ kN/m
M5	$L = H = 10.0$	$P = 5880$ kN
M6	$L = H = 10.0$	$P = 3820$ kN
M7	$L = H = 10.0$	$P = 25.7$ kN, $w = 129$ kN/m
M8	$L = H = 10.0$	$w = 143$ kN/m
M9	$L = H = 10.0$	$P = 2940$ kN
M10	$L = H = 10.0$	$P = 2310$ kN
M11	$L = H = 10.0$	$P = 5890$ kN
M12	$L = H = 10.0$	$w = 150$ kN/m
M13	$L_1 = 5.00, L_2 = 10.0, H = 10.0$	$P = 5880$ kN
M14	$L_1 = 5.00, L_2 = 10.0, H = 10.0$	$w = 155$ kN/m
M15	$L = H = 10.0$	$P = 2940$ kN
M16	$L = H = 10.0$	$P = 59.9$ kN, $w = 150$ kN/m
M17	$L = 9.14, H = 4.57$	$P = 1550$ kN, $W = 155$ kN
M18	$L_1 = 7.32, L_2 = 5.49, H_1 = 3.66, H_2 = 2.44$	$w = 95.8$ kN/m, $W_1 = 10.4$ kN, $W_2 = 15.8$ kN
M19	$L_1 = 6.10, L_2 = 14.6, H_1 = 6.10, H_2 = 4.57$	$w_R = 69.1$ kN/m, $w_F = 148$ kN/m
M20	$L = 6.10, H = 4.57$	$w_R = 27.6$ kN/m, $w_F = 59.2$ kN/m, $W = 7.62$ kN
M21	$L = 6.00, H = 3.75$	$w_R = 32.0$ kN/m, $w_F = 49.4$ kN/m, $W_R = 10.3$ kN, $W_F = 20.6$ kN

2.1. Modelling approach

2.1.1. Basic modelling assumptions

Geometrically and materially nonlinear analyses with imperfections (GMNIA) were performed to calculate the ultimate capacities of the studied frames. The two-noded linear Timoshenko beam element for open sections, denoted as B31OS in Abaqus [14] and capable of modelling transverse shear and warping deformations, was used in all simulations; 33 section points were specified along each flange and web plate to capture the stress distribution within the cross-sections accurately. The beam-column connections of the studied frames were assumed to be fully rigid. To reflect this, the physical size of the joint region, which depends on the cross-section depths of the adjoining members, was represented using *MPC BEAM constraints [14] as shown in Fig. 2a. Since in-plane stability design is the focus of the present study, deformations in the out-of-plane direction were restrained at all nodes of the developed FE models. The element length e_L was determined according to Eq. (1); this length was chosen to ensure that a minimum of three full elements lay within the minimum elastic local buckling half-wavelength of the modelled cross-sections for the implementation of the strain averaging approach (see Section 2.2). Model verification [11] was ensured through previous experience on the appropriate choice of element type for the studied problem and a prior mesh density study [1].

$$e_L = 0.3\min\left(L_{b,cs}^C, L_{b,cs}^B\right) \text{ but } e_L \leq L/40 \qquad (1)$$

Here, $L_{b,cs}^C$ and $L_{b,cs}^B$ are the elastic cross-section local buckling half-wavelengths under uniform compression and pure bending, respectively, as determined using the expressions provided in [17] and L is the member length.

2.1.2. Material modelling

The quad-linear material model developed by Yun and Gardner [18] was utilised to represent the full stress-strain behaviour of the simulated hot-rolled steel members. A Young's modulus E value of 200000 N/mm^2
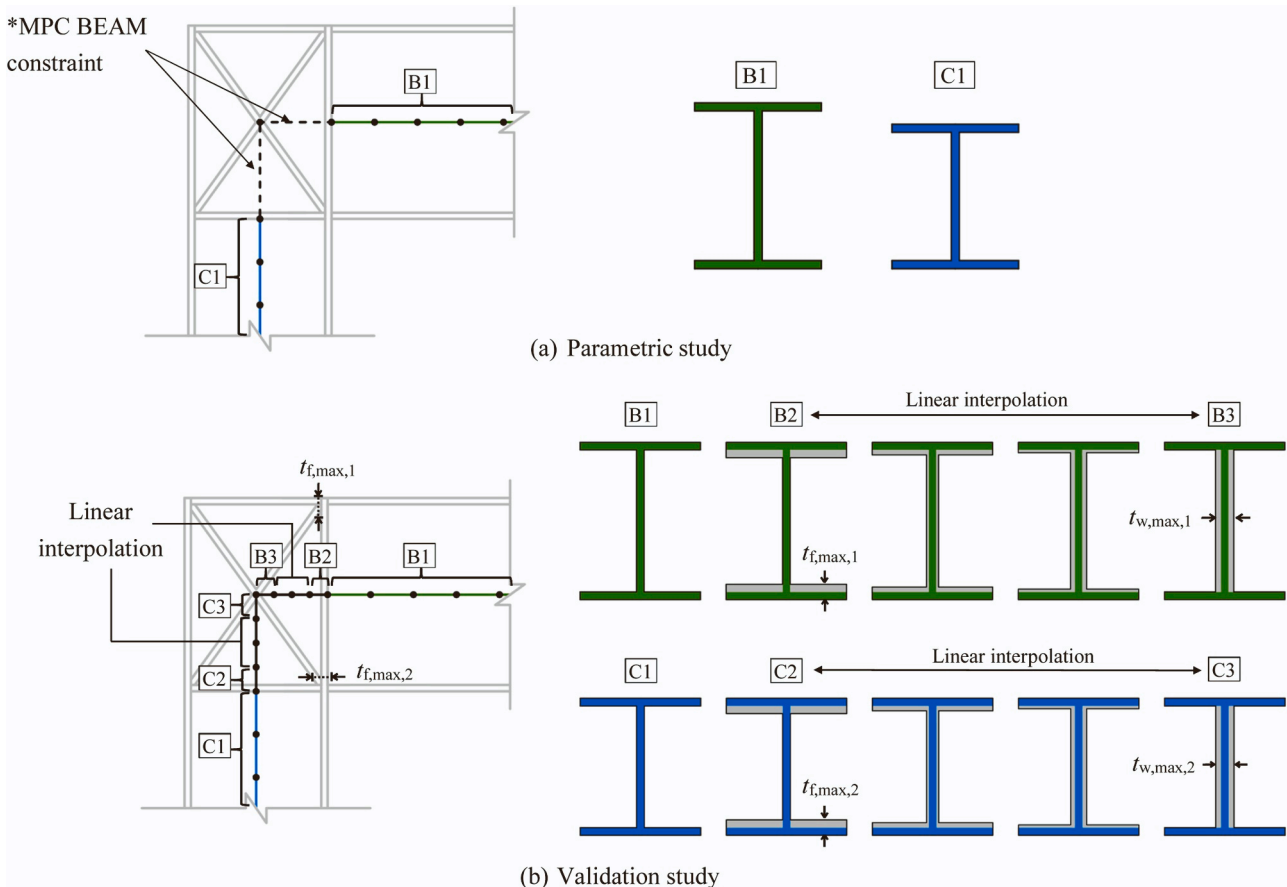

(a) Parametric study

(b) Validation study

Fig. 2. Modelling of joint region in the beam FE models utilised in (a) parametric study and (b) validation study.

and yield stress f_y value of 355 MPa were employed; the additional material parameters required for the definition of the quad-linear model were calculated using the expressions provided in [18]. In addition, the ultimate stress f_u was determined using the expression given in Eq. (2) [19]:

$$f_u = f_y \left[1 + \left(\frac{200}{f_y} \right)^{1.75} \right] \quad (2)$$

The material properties were introduced into Abaqus [14] in the format of true stress σ_{true} - true plastic strain ε_{true}^{pl} [6], which can be obtained according to Eqs. (3) and (4),

$$\sigma_{true} = \sigma(1 + \varepsilon) \quad (3)$$

$$\varepsilon_{true}^{pl} = \ln(1 + \varepsilon) - \frac{\sigma_{true}}{E} \quad (4)$$

where σ and ε are the engineering stress and strain, respectively.

2.1.3. Geometric imperfections and residual stresses

Residual stresses can be modelled either explicitly by assigning initial stress values to each section point of the cross-section through the SIGINI user subroutine [14] or implicitly by the use of equivalent geometric imperfections. For ease of modelling, the latter approach was adopted throughout the parametric study, both in determining the benchmark worst case imperfection and in the establishment and assessment of the imperfection definition methods – see Section 3.1. Residual stresses were modelled explicitly in the validation study to achieve the most accurate replication of the experimental data – see Section 2.3.

2.2. Cross-section resistance

In GMNIA, the effects of frame and member instabilities are directly accounted for, thereby eliminating the need for subsequent member checks. However, instabilities at the cross-section level such as local buckling cannot be captured by beam elements. Therefore, additional measures are necessary to avoid overprediction of ultimate capacity. Traditionally, cross-section classification and the associated cross-section checks are utilised. In the present study, the effects of local buckling are accounted for more accurately by the application of strain limits [1,6,7,20]. The strain limit ε_{csm} prescribes the level of deformation a cross-section can endure failure and is calculated from the Continuous Strength Method (CSM) [21–23] base curve, as given by Eqs. (5) and (6) for non-slender and slender cross-sections, respectively:

$$\frac{\varepsilon_{csm}}{\varepsilon_y} = \begin{cases} \dfrac{0.25}{\overline{\lambda}_p^{3.6}} \text{ but } \leq \Omega & \text{for } \overline{\lambda}_p \leq 0.68 \quad (5) \\[2ex] \left(1 - \dfrac{0.222}{\overline{\lambda}_p^{1.05}} \right) \dfrac{1}{\overline{\lambda}_p^{1.05}} & \text{for } 0.68 < \overline{\lambda}_p \leq 1.00 \quad (6) \end{cases}$$

where ε_y is the yield strain, Ω provides an upper bound to the permissible level of plastic deformation, with a value of 15 used herein, and $\overline{\lambda}_p$ is the cross-section slenderness defined by Eq. (7):

$$\overline{\lambda}_p = \sqrt{\frac{f_y}{\sigma_{cr,cs}}} \quad (7)$$

where f_y is the yield stress and $\sigma_{cr,cs}$ is the elastic local buckling stress of the full cross-section. In the present study, $\sigma_{cr,cs}$ is determined using the simplified expressions developed in [24]. The adverse influence of high shear (i.e. when $V_{Ed}/V_{pl,Rd} > 0.5$, where V_{Ed} is the design shear force and $V_{pl,Rd}$ is the plastic shear resistance) on bending capacity is accounted for by the calculation of a reduced strain limit $\varepsilon_{csm,V}$ [25].

The CSM strain limit ε_{csm} depends on the slenderness of the cross-section $\overline{\lambda}_p$, which in turn is a function of $\sigma_{cr,cs}$, with $\sigma_{cr,cs}$ depending on the stress distribution acting on the cross-section; this stress distribution will generally vary throughout the analysis due to geometric and material nonlinearities. The instantaneous stress distribution determined at every increment in the numerical analysis was therefore used to calculate ε_{csm}. Additionally, the beneficial effects associated with local moment gradients on the strength and stability of cross-sections were allowed for by averaging the compressive strains over the elastic local buckling half-wavelength $L_{b,cs}$ [1]. The failure load was then defined as the first to occur of (1) the peak load and (2) the load at which the average outer fibre compressive strain over the cross-section elastic local buckling half-wavelength reached the corresponding strain limit.

2.3. Validation

The modelling approach described in Section 2.1, along with the cross-section failure criterion presented in Section 2.2, were validated against the experimental results from tests on 10 moment frames; two full scale frames presented in [26] and eight quarter scale frames (four single-storey and four two-storey) presented in [27]. To ensure comparability between the numerical results obtained from the established FE models and the experimental results, the measured material properties and cross-section dimensions were used as the FE model input parameters. Note that where different material properties in the flanges and webs were reported, weighted average material properties representative of the entire cross-section were utilised [6,28]. Where the full stress-strain relationship of the tested material was not provided, the quad-linear material model described in Section 2.1.2 was used. Both geometric imperfections and residual stresses were considered explicitly. The ECCS [29] residual stress patterns for hot-rolled sections were assumed. Since no information on geometric imperfections was provided in the considered studies, the initial imperfection shape was defined according to Fig. 3 (mirroring the recommendations of DD1 – see Section 4.1.1), with the imperfection amplitudes chosen as $L/1000$ for the bow component and $H/500$ for the sway component based on the manufacturing and erection tolerances in [30]. The sway imperfections were applied only in the in-plane direction while bow imperfections were applied in both the in-plane and out-of-plane directions. The locations of the out-of-plane restraints and the loading sequence, as reported in the experimental studies, were replicated in the numerical simulations.

The strength and stiffness of the studied beam-column connections [26,27] were considered in the FE models by adopting the joint modelling approach depicted in Fig. 2b. This involved assigning increased flange thicknesses of $t_{f,max,1}$ and $t_{f,max,2}$ to the elements in the joint region immediately next to the adjoining beam (element B2) and column (element C2), respectively. Additionally, the elements adjacent to the frame corner (elements B3 and C3) were assigned increased web thicknesses of $t_{w,max,1}$ and $t_{w,max,2}$ such that the modified cross-sectional area was equal to that of the corresponding compound 3-flange cross-section at the centre of the joint region. The flange and web thicknesses of the remaining elements within the joint region were then determined from linear interpolation. Note that in all cases only the thickness of the flange and/or web was modified (i.e. with no change to the height or width of the section). Since this type of beam-column connection provides significant resistance to warping deformations [31], the warping degree of freedom was restrained at the node where the beam and column intersect. The rigidity of the frame base supports was accounted for by means of rotational springs with a stiffness of $k_\theta = 5.7 \times 10^4$ kNm/rad for the two full scale frames [26] and $k_\theta = 3.3 \times 10^4$ kNm/rad for the eight quarter scale frames [27], as calculated in [28].

A summary of the validation study results is provided in Table 2. Overall, accurate strength predictions were obtained from the developed
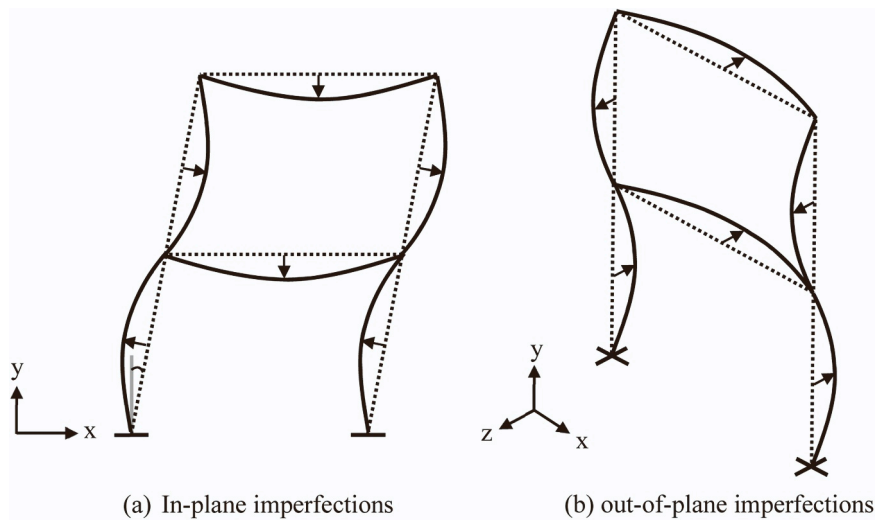
(a) In-plane imperfections   (b) out-of-plane imperfections

Fig. 3. Assumed imperfection shape for (a) in-plane and (b) out-of-plane imperfections for frame FE validation models.

FE models, with a mean FE-to-test ultimate load ratio of 0.90 and a coefficient of variation (CoV) of 0.02. The slight average under-prediction of the test ultimate capacities is attributed to some un-certainties in the joint characteristics and material properties and some conservatism in the CSM strain limits, as mentioned below. Note that all frames presented in [26] and [27] were unloaded upon the attainment of a predefined horizontal displacement. For the tests in which the ultimate capacity was not reached, the maximum applied load prior to the unloading stage was considered as the ultimate capacity.

In Fig. 4, the load-displacement responses predicted from the developed FE models are compared against the experimental results for the two full scale frames (specimens FM0 and FM5) presented in [26], where H is the applied horizontal load, P is the applied vertical load and Δ is the horizontal displacement of the right-hand joint at the top storey. Specimen FM0 was subjected to horizontal loading only, while specimen FM5 was loaded vertically to a predefined load level before being loaded horizontally to failure. The overall responses of both frames are accu-rately captured by the developed FE models, with the bending domi-nated specimen FM0 experiencing a significant degree of strain hardening and the stability governed specimen FM5 exhibiting a clear peak followed by softening behaviour. For specimen FM5, it was found that the direction of the sway imperfection had a notable impact on the predicted ultimate load due to the compression dominated loading. The results for specimen FM5 presented in Fig. 4 and Table 2 were thus obtained with the sway imperfection applied in the opposite direction to the applied horizontal load (i.e. negative x-direction in Fig. 3), since it was found to provide a closer response to that seen in the experiment.

For the quarter scale frames presented in [27], the developed FE models were able to capture the ultimate loads accurately for all the single-storey SI series frames. However, the failure loads for the two-storey SII series frames were consistently underestimated. Fig. 5

Table 2
Comparison of numerical and experimental ultimate capacities (FE/Test) for 10 moment frames [26,27].

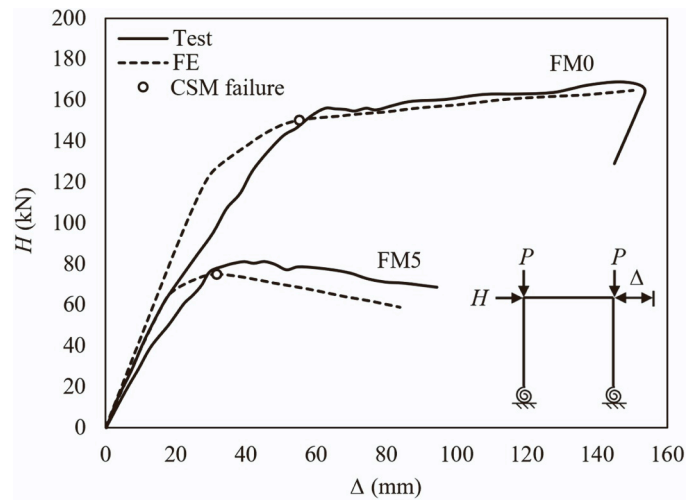| Type of structure	Reference	No. of tests	FE/Test	
			Mean	CoV
Moment frame (single-storey)	Wakabayashi et al. [26]	2	0.90	0.02
	Wakabayashi & Matsui [27]	4	0.94	0.03
Moment frame (two-storey)	Wakabayashi & Matsui [27]	4	0.84	0.02
	Total	10	0.90	0.02

Fig. 4. Validation of beam FE models against the experimental results of two full scale single storey moment frames (specimens FM0 and FM5) reported in [26].

shows the experimental load-displacement responses for specimens SI-1, SI-3 and SII-1 together with the corresponding FE predictions. For the SI frames, the numerical and experimental results show excellent agree-ment for both the initial stiffness and the failure load. The FE models accurately captured the more pronounced development of strain hard-ening in specimen SI-3 than in specimen SI-1 due to the stiffer restraint provided to the columns by the adjoining beam. However, for specimen SII-1, the FE model predicted the initial stiffness accurately, but underestimated the failure load. This is thought to be owing to the discrepancy between the material properties employed in the FE models and the actual values of the tested specimen. Analytical plastic hinge analyses which consider the effects of strain hardening and rigid joint regions were also performed on the tested frames in [16]; the strengths for all the SII series frames were again underestimated.

3. Most severe imperfection shapes

In this section, the most severe imperfection shape for each of the investigated frame configurations was sought. For this purpose, an imperfection combination study was carried out, as presented in Section 3.2, in which each frame configuration was analysed for every possible
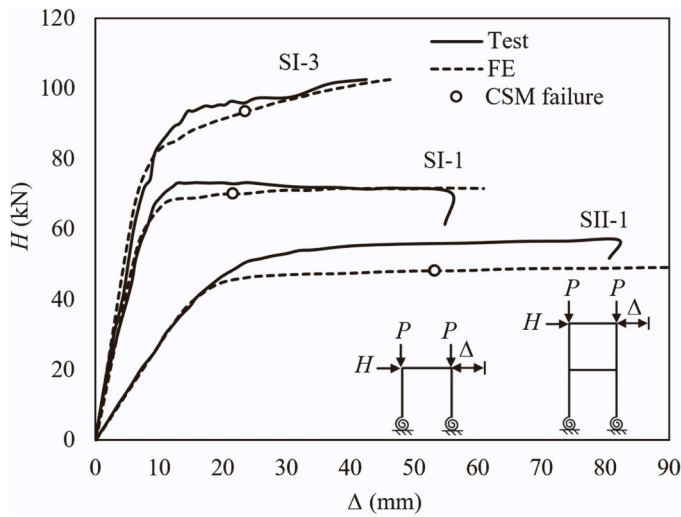
Fig. 5. Validation of FE models against experimental results of single-storey (SI-1, SI-3) and two-storey (SII-1) quarter scale moment frames reported in [27].

combination of imperfection directions. Additionally, a variance-based sensitivity analysis was carried out, as presented in Section 3.3; this analysis identifies which aspects of an imperfection has the largest impact on the ultimate capacity and provides information on how the ultimate capacity varies with the amplitude of the imperfection. The described studies were conducted using Python [32] from which the '.inp' files were written and an interface with Abaqus was established. To accommodate the large number of numerical analyses, the jobs were placed into a centralised queue and distributed out to clusters of computers. On each computer, multiple instances of Abaqus were run in parallel and the subsequent CSM design checks were performed. This approach enabled approximately 30000 analyses to be run per day across 125 computers.

3.1. General

The definition of geometric imperfections relies on both the imperfection shape and the imperfection amplitude. These variables can be considered independently as further explained in the following sections.

3.1.1. Imperfection shape

For stability design, the shape of the imperfection should be defined such that it provides the greatest destabilising effect (i.e. the imperfection shape that minimises the ultimate capacity of the frame) [9], referred to herein as the most severe imperfection shape. The process of identifying this shape is non-trivial since the ultimate capacity depends upon several factors including the material, geometry, connectivity, boundary conditions and applied loading. For planar frames, it is common for the imperfection to be split into two component imperfections, namely: (1) sway or out-of-plumbness imperfections, which describe the imperfections at the connections between the members, and (2) bow or out-of-straightness imperfections, which define the imperfections within the members.

The sway imperfections are modelled herein as horizontal displacements, while the bow imperfections are modelled as a half-sine wave along the length of each member. As such, the imperfection shape can be characterised entirely in terms of a direction vector $\boldsymbol{x}$, which consists of elements of either -1, 0 or 1 depending upon the direction in which the corresponding sway or bow imperfection applies. Thus, the elements of the direction vector can be expressed as $x_i \in \{-1,0,1\}$ for $i = 1,\ldots,$ $n_{\mathrm{J}},\ldots,n_{\mathrm{J}}+n_{\mathrm{B}},\ldots,n_{\mathrm{J}}+n_{\mathrm{B}}+n_{\mathrm{C}}$ where n_{J}, n_{B}, and n_{C} represent the number of joints, beams, and columns, respectively. The number of members n_{M} is given by $n_{\mathrm{M}} = n_{\mathrm{B}} + n_{\mathrm{C}}$.

3.1.2. Imperfection amplitude

The imperfection amplitude is described in terms of the magnitudes of the initial displacements at key points throughout the frame. The imperfection amplitude can be characterised by an amplitude vector $\boldsymbol{a}$ of size equal to the direction vector with the elements a_i equal to the amplitude of the corresponding sway or bow imperfection. The amplitude of a given sway imperfection at a joint is expressed as the absolute value of the horizontal displacement relative to the joint that lies directly below it, and the amplitude of a given bow imperfection is defined as the maximum of the absolute value of the displacements along the length of the member relative to the centreline of the member projected into the direction normal to the member.

Accompanying the amplitude vector is the amplitude limit vector $\overline{\boldsymbol{a}}$ and an imperfection utilisation vector $\boldsymbol{U}_{\mathrm{I}}$. The former allows the designer to prescribe upper bound limits on the amplitudes observed throughout the frame, while the latter provides an intuitive way of measuring the imperfection amplitude with reference to these limits. The choice of $\overline{\boldsymbol{a}}$ is established herein based upon equivalent imperfection amplitudes with the member bow imperfection limit taken as the greater of $\alpha L/150$ (where α is the imperfection factor [33] and L is the member length) and $L/1000$ [34], and the sway imperfection limit taken as $H_{\mathrm{s}}/400$ [13,33], where H_{s} is the height between consecutive storeys. The imperfection utilisation vector consists of elements $U_{\mathrm{I},i} = a_i/\overline{a}_i$ for $i = 1,\ldots,n_{\mathrm{J}}+n_{\mathrm{M}}$ that provide a non-dimensional utilisation, indicating how close each amplitude a_i is to its corresponding limit $\overline{a}_i$. The imperfection utilisation vector is useful for summarising certain characteristics and features of an imperfection, with, for example, its average value (i.e. mean($\boldsymbol{U}_{\mathrm{I}}$)) providing a suitable one-dimensional measure of the amplitude across the entire frame. The imperfection utilisation vector can also be split into two parts, $\boldsymbol{U}_{\mathrm{I,sw}}$ and $\boldsymbol{U}_{\mathrm{I,ns}}$, corresponding to the separate imperfection utilisation of the sway and non-sway (i.e. bow) imperfections, respectively. A summary of the concepts introduced in this section is presented graphically in Fig. 6.

3.2. Imperfection combination study

An imperfection combination (IMC) study was carried out to determine the most severe imperfection shape for each of the considered frames, as summarised in Fig. 7. The imperfections were defined using the direction vector and amplitude vector, as discussed in Sections 3.1.1 and 3.1.2, respectively. It was assumed herein that all joints and members existed in their imperfect form and thus the elements of the direction vector were reduced to $x_i \in \{-1,1\}$ for $i = 1,\ldots,n_{\mathrm{J}}+n_{\mathrm{M}}$. With the focus of the IMC study relating to the imperfection shape, the imperfection amplitude was kept constant. The amplitude vector was set equal to the recommended amplitude limit vector, as discussed in Section 3.1.2, and thus the imperfection utilisation vector was given by $U_{\mathrm{I},i} = 1.0$ for $i = 1,\ldots,n_{\mathrm{J}}+n_{\mathrm{M}}$. The ultimate load factor for each frame associated with the most severe imperfection shape is defined as the benchmark ultimate load factor α_{u} and will be used in Section 5 when evaluating the performance of the different methods for defining imperfections.

The IMC study itself consisted of trialling all possible sway-member imperfection combinations that could exist by varying the contents of the direction vector. Each element of the direction vector falls into one of two states, therefore the total number of imperfection combinations that exist for a given frame is expressed as $2^{n_{\mathrm{J}}+n_{\mathrm{M}}}$. For Frames M1 to M19, all possible imperfection combinations were assessed. However, for Frames M20 and M21, this would have resulted in 8.39×10^6 and 2.81×10^{14} numerical simulations, respectively; therefore, to reduce the excessive computational costs, the number of examined imperfection combinations for Frames M20 and M21 were strategically reduced using the results of the imperfection combination study across Frames M1 to M19. This involved confining the direction of the bow imperfections in Frames M20 and M21 to induce sagging in the beams (i.e. $x_i = -1$ for $i = n_{\mathrm{J}}+1,\ldots,n_{\mathrm{J}}+n_{\mathrm{B}}$). Additionally, for Frame M21,
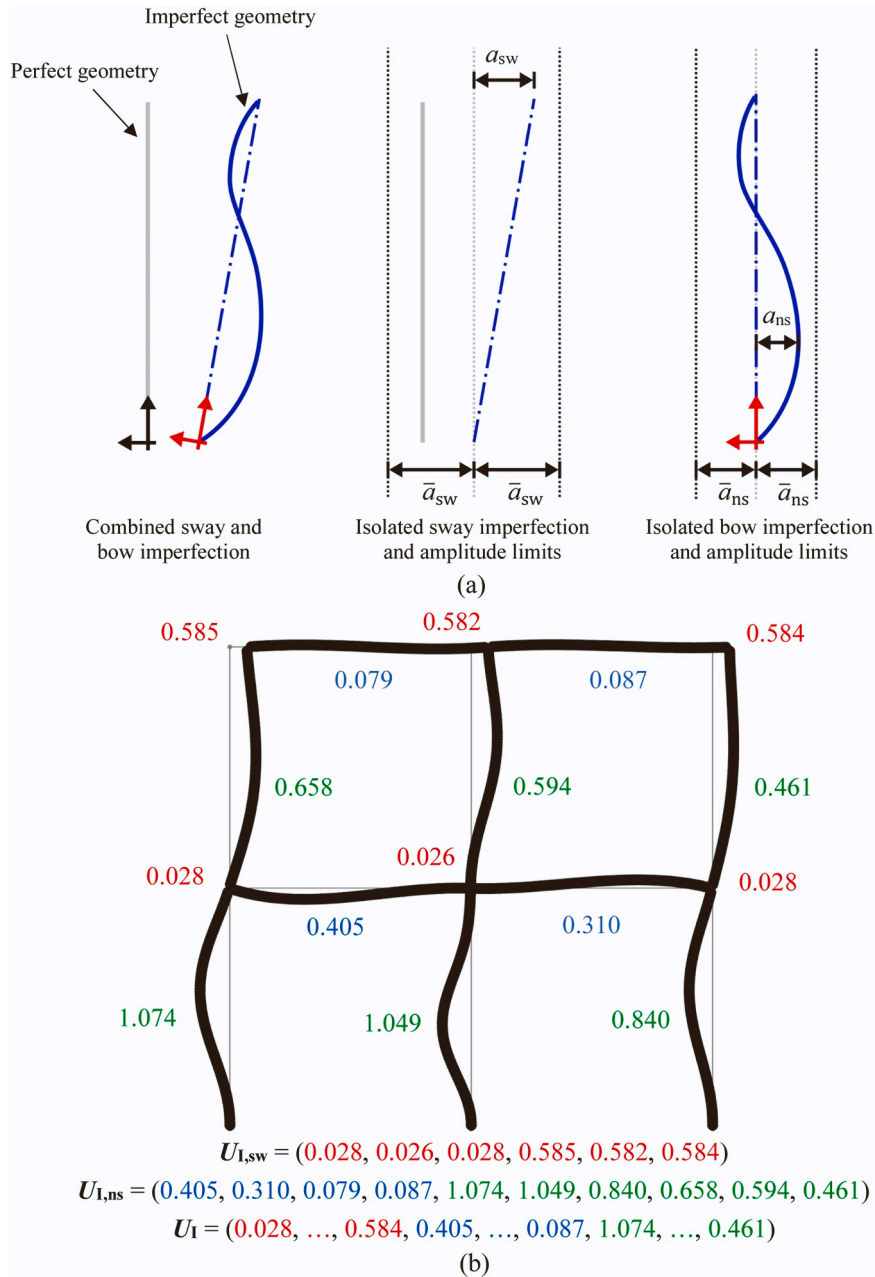
Fig. 6. Graphical illustration of (a) how to measure the amplitude (a_{sw} and a_{ns}) and amplitude limit ($\bar{a}_{sw}$ and $\bar{a}_{ns}$) corresponding to a given sway and bow imperfection in a typical member (b) the imperfection and imperfection utilisation vector U_I associated with Frame M16 using the eigenmode-based method EM3-B alongside a breakdown of U_I into separate sway $U_{I,sw}$ and bow $U_{I,ns}$ components.

several terms within the direction vector were grouped together resulting in six groups of sway directions (comprising three joints each – labelled 1–6 in red on Fig. 7) and three groups of bow directions (comprising six columns each, one group for each line of columns – labelled 1–3 in green on Fig. 7). The directions of the sway imperfections within the sway groups were defined such that the assigned sway direction, either positive or negative, was the same across the entire group, while the imperfection directions of the columns within the column groups were defined according to one of four possible states: (1) all imperfections in the negative direction, (2) the first storey column imperfection in the negative direction and alternate going upwards, (3) the first storey column imperfection in the positive direction and alternate going upwards, or (4) all imperfections in the positive direction. Following these assumptions, the total number of imperfection combinations for Frames M20 and M21 were significantly reduced to $2^{n_J+n_C}$

$= 2^{9+9} = 262144$ and $2^6 4^3 = 4096$, respectively. It should be noted that since only a subset of imperfections were considered for Frames M20 and M21, the most severe imperfection shapes determined may not be the most severe possible; however, it is expected that the corresponding benchmark ultimate load will be very close to that of its true value.

Fig. 7 provides an overview of the results from the IMC study, in which the most severe imperfection shape, the number of considered imperfection combinations n_{IMC}, the benchmark ultimate load factor α_u and governing failure criterion are presented for each frame. In total, 467232 numerical simulations were conducted for the IMC study. As illustrated in Fig. 7, different characteristics in the most severe imperfection shapes can be observed depending upon the failure mode of the frame. The frames that failed through instability (i.e. at the peak load) typically had all sways acting in the same direction, and in sympathy with the direction of lateral loading, where present. The cross-section
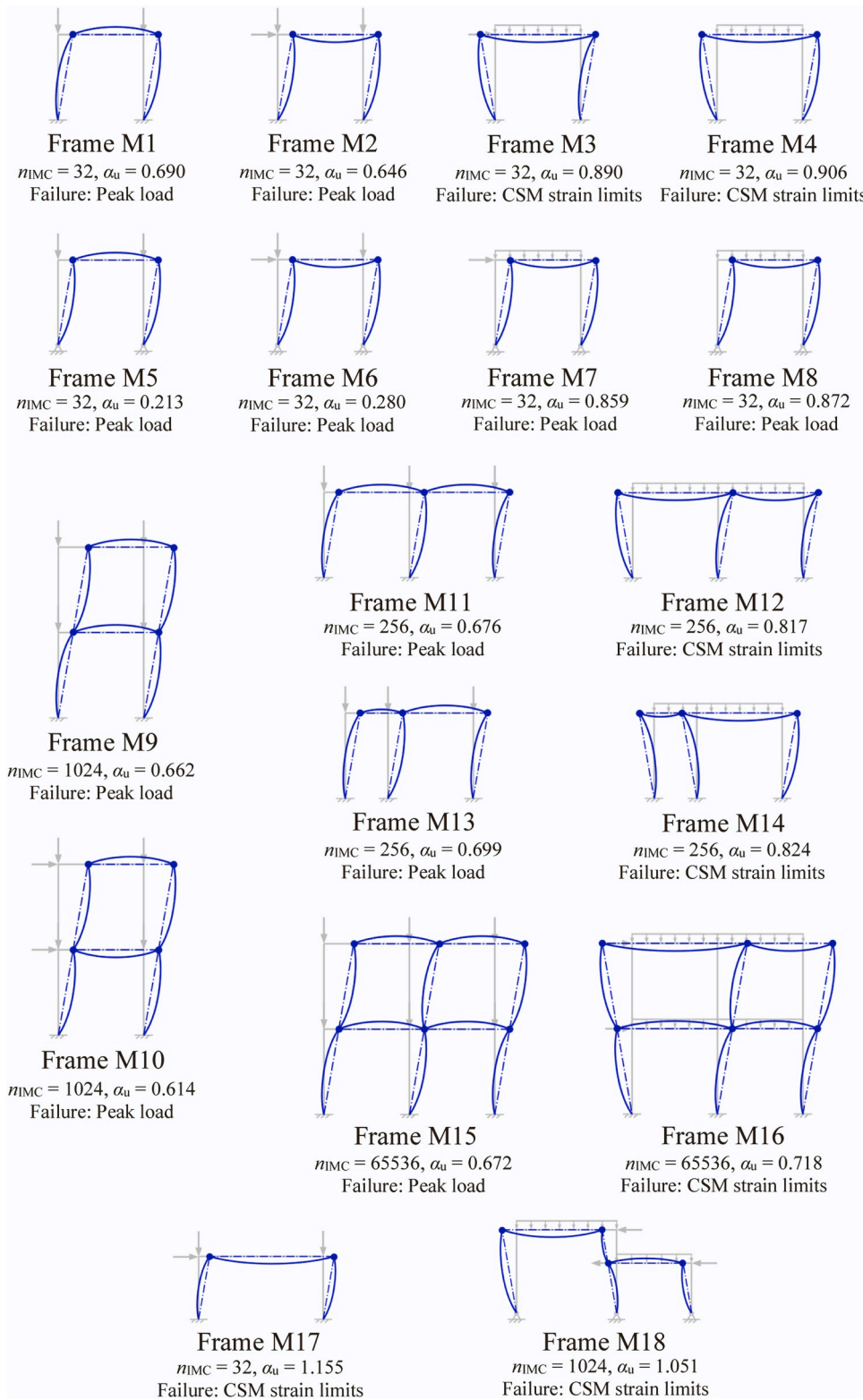
Fig. 7. Most severe imperfection shapes determined for considered moment frame, where n_{IMC} indicates the number of imperfection shapes examined and α_u is the benchmark ultimate load factor. Note that the members and joints for which both positive and negative imperfection directions were examined are shown in blue while those with a fixed imperfection direction are shown in black. For Frame M21, the red and green represent the six sway groups and three column groups, respectively.

strength-governed frames (the resistance of which was controlled by the CSM strain limits), on the other hand, typically established the sways such that they lengthened the member within which the CSM failure occurs; by lengthening the member, the midspan bending moment is increased which leads to larger strains, thus reaching the CSM strain limit earlier. Finally, greater variance was observed in the ultimate
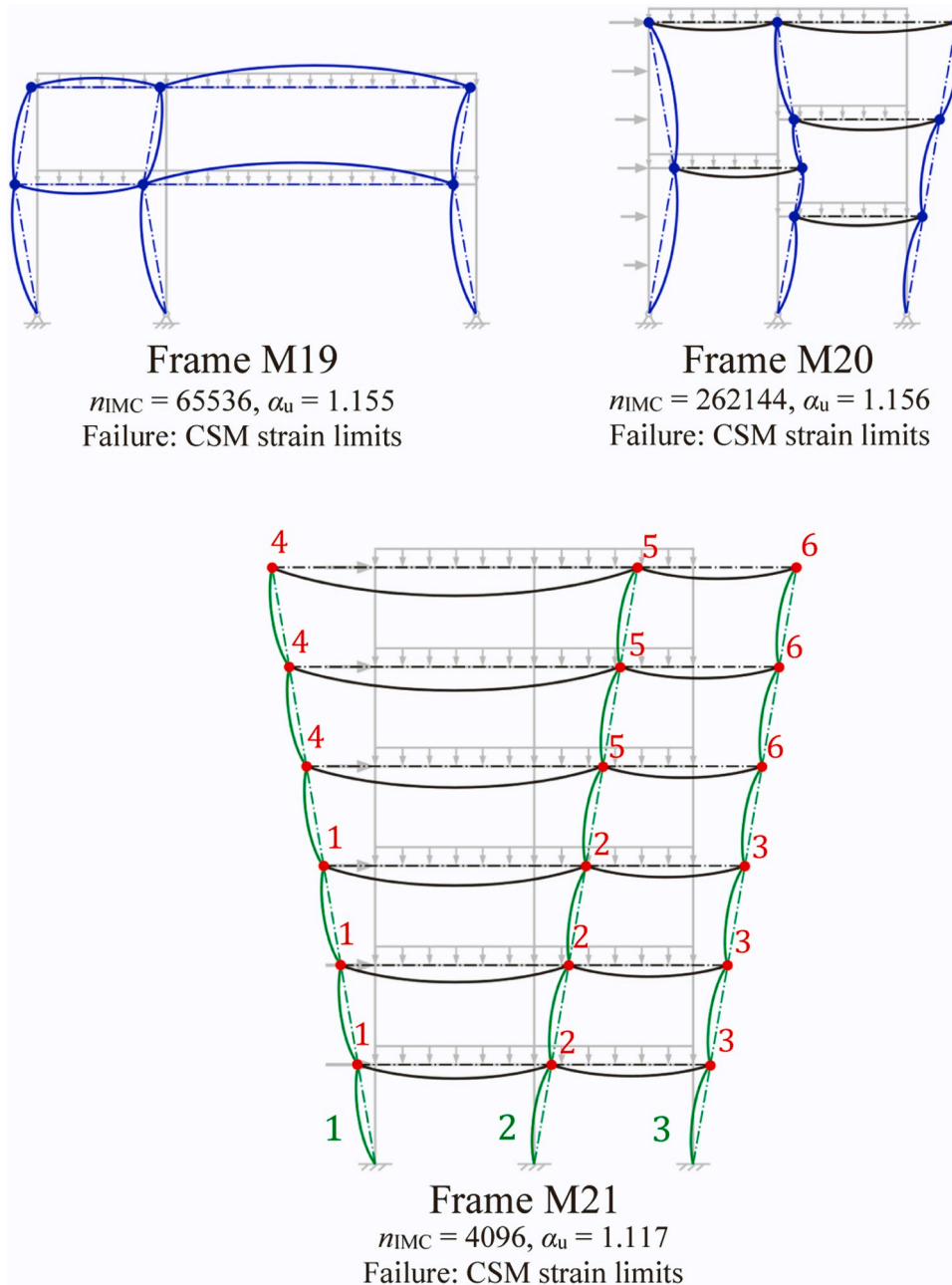
Frame M19

$n_{\text{IMC}} = 65536$, $\alpha_u = 1.155$
Failure: CSM strain limits

Frame M20

$n_{\text{IMC}} = 262144$, $\alpha_u = 1.156$
Failure: CSM strain limits

Frame M21

$n_{\text{IMC}} = 4096$, $\alpha_u = 1.117$
Failure: CSM strain limits

Fig. 7. (*continued*).

capacities of the stability-governed rather than strength-governed frames. This confirms, as expected, that the strength-governed frames are relatively imperfection insensitive. Therefore, when proposing the strategy for defining imperfections, greater consideration was given to including the characteristics of the most severe imperfection shapes from the frames that were stability-governed.

3.3. Variance-based sensitivity analysis

Variance-based sensitivity analysis (VAR), also known as Sobol's method [35], is a method of global sensitivity analysis that provides a means of obtaining fractional contributions (i.e. sensitivities) to the variance in the output of a mathematical model characterised according to which group of inputs are being considered. In this context, the output is taken as the ultimate capacity of the frame, with the inputs being the imperfection amplitude and shape. To compute these sensitivities, one is

required to sample many imperfections of varying amplitude and shape. The more samples that are taken, the more accurate the computed sensitivities become. While for many studies the focus is on computing and interpreting these sensitivities, the VAR is used herein primarily as a means of generating an additional set of data points to aid in understanding how the amplitude and shape affect the ultimate capacity, but by sampling in a particular way, such as via a Sobol sequence [35], sensitivities can be obtained as a by-product. Using the estimators provided in [36], the total-effect sensitivities associated with each component i of the imperfection were computed. These sensitivities represent the overall effect that a given component i has on the ultimate capacity of the frame; the values range from 0.0 to 1.0, with higher values indicating greater influence. To compute each total-effect sensitivity, $n_s = 1024$ samples were taken, resulting in a total of $n_s(d + 2)$ samples per frame where $d = n_J + n_M$. In total, 274432 numerical simulations were conducted for the VAR. Further details on the approach to computing

these sensitivities can be found in [37].

The findings of the VAR were two-fold. Firstly, as shown in Table 3, which provides the average total-effect sensitivities by variable type, the sway imperfections were observed to be most significant, followed by the bow imperfections in the columns, and finally the bow imperfections in the beams. This would indicate that when developing a strategy for defining imperfections, particular care should be taken to ensure that the sway imperfections are being defined correctly. Relatively low sensitivity to member bow imperfections would be anticipated in moment frames since all members, including the columns, experience significant bending actions, with the resulting deflections serving a similar role to the imperfections in amplifying the instability effects of the compressive loads. Such behaviour would not generally be seen in braced frames since the columns typically experience very little bending. Secondly, assuming that the imperfection shape has been chosen appropriately, the ultimate capacity decreases with increasing amplitude. This can be seen in Fig. 9, in which the normalised ultimate load is plotted against mean(U_I) for Frames M1 and M2. Since the imperfection amplitude was kept constant during the IMC study, the associated data points lie on the line mean(U_I) = 1.0, while the data points associated with the VAR lie between mean(U_I) = 0.0 and mean (U_I) = 1.0. The effect of imperfection shape is observed through the spread of the data vertically. Clearly defined bands corresponding to the different combinations of sway and bow directions can be observed within the results of the IMC study and, to a lesser extent, within the results of the VAR. Additionally, the symmetry of Frame M1 and its lack of lateral loading can be seen in the results of Fig. 9, where both positive and negative sway imperfections cause the ultimate load to decrease, unlike with Frame M2 where only positive sway imperfections (i.e. those aligned with the direction of lateral loading) cause a reduction in the ultimate load.

4. Imperfection definition methods

In this section, the two approaches considered herein for introducing initial geometric imperfections into FE models – direct definition-based and eigenmode-based – are outlined. The direct definition-based methods DD1 and DD2 are introduced in Section 4.1, while the

Table 3
Results from VAR indicating total-effect sensitivities averaged by variable type for each of the considered frames.

Frame	Average total-effect sensitivities by variable type		
	Sways	Beams	Columns
M1	0.821	0.000	0.162
M2	0.482	0.000	0.020
M3	0.421	0.044	0.057
M4	0.467	0.053	0.007
M5	0.226	0.000	0.113
M6	0.376	0.000	0.124
M7	0.446	0.003	0.052
M8	0.688	0.004	0.180
M9	0.462	0.001	0.115
M10	0.238	0.000	0.014
M11	0.612	0.000	0.131
M12	0.295	0.007	0.295
M13	0.609	0.000	0.101
M14	0.272	0.017	0.050
M15	0.335	0.000	0.076
M16	0.117	0.005	0.047
M17	0.492	0.000	0.007
M18	0.177	0.000	0.073
M19	0.135	0.003	0.029
M20	0.091	0.000	0.019
M21	0.053	0.002	0.004
Min.	0.053	0.000	0.004
Mean	0.372	0.007	0.080
Max.	0.821	0.053	0.295
CoV	0.545	2.113	0.883

eigenmode-based methods EM1, EM2, and EM3 are introduced in Section 4.2. The key aspects of all five methods are summarised in Table 4.

4.1. Direct definition-based methods

In this section, the two direct definition-based methods considered herein, DD1 and DD2, are detailed. These methods require the designer to directly modify the nodal coordinates of the FE mesh and result in imperfections akin to those of the IMC study. The direction vector, as introduced in Section 3.1.1, is obtained from the chosen direct definition-based method, while the amplitude vector is assumed constant, with amplitudes equal to their corresponding limits, as described in Section 3.1.2.

4.1.1. DD1

The rules for defining the directions of the sway and bow imperfections in DD1 are summarised in Table 5, and were derived from the results of the IMC and VAR studies. The rules governing the directions of the sways were established primarily from the results of the IMC study, particularly for the stability-governed frames. The rules governing the directions of the bow imperfections on the beams were based upon the findings of the VAR, from which it was deduced that the imperfections in the beams had the lowest impact on the ultimate capacity, and thus a sagging direction was adopted throughout; this is both convenient and will, in most circumstances, match the direction of the applied loading. The rules governing the directions of the bow imperfections in the columns were deduced by considering the results from the IMC study and observing how the ultimate capacity changes depending upon the chosen column imperfection definition strategy. The considered column arrangements were the same as those outlined in Section 3.2 for Frame M21. These results are provided in Table 6, where it is shown that alternating the direction of the column imperfections from storey-to-storey, with the imperfection direction in the first storey columns being established based upon the direction of the sways and the boundary conditions, yields the best results overall.

4.1.2. DD2

In DD2, the directions of the sway and bow imperfections are inferred from the eigenmodes of an LBA (see Section 4.2). The first sway and first non-sway modes are used to determine the directions of the sway and bow imperfections, respectively. Where the direction of the bow imperfection in a given member is ambiguous, higher order non-sway modes may be used. An eigenmode is classified as a sway mode if the maximum displacement occurs at one of the connections between the members, otherwise it is classified as a non-sway mode, with the maximum displacement being located within the length of one of the members. The direction of the first sway and first non-sway modes were chosen according to the rules governing the choice of eigenmode direction set out in Section 4.2. This direct definition-based method mirrors the provisions of [33], in which it is stated that 'the assumed shape of sway and bow imperfections may be derived from the elastic buckling modes of a structure in the plane of buckling considered.'.

4.2. Eigenmode-based methods

In this section, the three eigenmode-based methods considered herein are detailed, as summarised in Table 4. These methods utilise eigenmodes obtained from an LBA imported as geometric imperfections into a subsequent FE model. Many FE software packages provide tools for importing and scaling these imperfections directly into the FE model, such as with the *IMPERFECTION keyword in Abaqus [14]. It is recommended to inspect (either visually or through an established automated procedure) the eigenmodes before importing to avoid the inclusion of spurious eigenmodes or those with negative eigenvalues. Such eigenmodes may not necessarily have a large impact on the structural response, but their presence could prevent other more

Table 4
Summary of methods for applying member and system level geometric imperfections considered herein.

Approach	Imperfection definition method	Shape of the imperfection	Illustration
Direct definition-based	DD1	Defined according to a proposed set of rules—see Table 5	
	DD2	Directions dictated by the critical sway and non-sway eigenmodes from LBA	
Eigenmode-based	EM1	Scaled critical eigenmode	
	EM2	Scaled superposition of the first six eigenmodes from LBA	
	EM3	Scaled superposition of the first sway mode and all non-sway modes for which the eigenvalues under the design loading satisfy $\alpha_{cr,ns} < 25$	

significant eigenmodes from contributing to the imperfection and have therefore been excluded herein. It should be also noted that eigenmodes can be arbitrarily scaled while still satisfying the eigenvalue problem. Hence, it is important to first understand how the eigenmodes have been normalised to ensure that the size of the applied imperfection is as intended. By default, Abaqus [14] normalises eigenmodes such that the maximum displacement is 1.0.

The direction of each eigenmode, as dictated by the sign of the associated scale factor, should be chosen such that it would be expected to cause a reduction in the ultimate capacity. The following set of rules governing the choice of eigenmode direction was adopted herein. The direction of the first sway mode was chosen such that it was in sympathy with the direction of the applied lateral loads. Where no lateral loads were present, the imperfections resulting from both positive and negative scale factors on the first sway mode were considered, with the imperfection that yielded the lowest ultimate capacity being representative of the considered imperfection definition method. The direction of the remaining modes (higher order sway modes and all non-sway modes) were defined as given by the LBA.

The imperfection associated with any given eigenmode-based method can be expressed as follows:

$$\boldsymbol{u_0} = V\boldsymbol{A} = \boldsymbol{v}_{m_1}A_{m_1} + \dots + \boldsymbol{v}_{m_k}A_{m_k} \tag{8}$$

where $V = \left[\boldsymbol{v}_{m_1}, \dots, \boldsymbol{v}_{m_k}\right]$ is a matrix whose columns consist of the ei-

genmodes corresponding to a mode selection vector given by $\boldsymbol{m} = (m_1, \dots, m_k)$, k is the number of eigenmodes used, and $\boldsymbol{A}$ is an accompanying set of scale factors. The adopted eigenmode-based method dictates the contents of V by specifying which eigenmodes are to be used to construct the imperfection. Once an eigenmode-based method has been chosen, one of two scaling options, A or B, can be applied, which in turn, alongside the rules for eigenmode direction, provide the set of scale factors $\boldsymbol{A}$. Combining an eigenmode-based method with a scaling option yields a uniquely defined imperfection represented by EMX-Y where X and Y indicate the chosen eigenmode-based method and scaling option, respectively. For example, EM1-A refers to an imperfection consisting of the eigenmodes selected according to EM1 and scaled according to scaling option A.
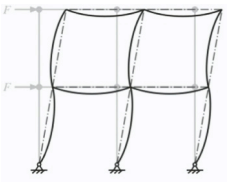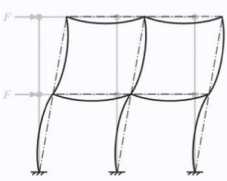
4.2.1. EM1

In EM1, only the first, and thus most critical, eigenmode is used. The selection vector is given by $\boldsymbol{m} = (1)$ which results in $V = \boldsymbol{v_1}$ and the accompanying $\boldsymbol{A}$ becomes a scalar.

4.2.2. EM2

The first six eigenmodes are used in EM2, as suggested in [38,39]. The selection vector is therefore given by $\boldsymbol{m} = (1,2,3,4,5,6)$ and hence $V = [\boldsymbol{v_1}, \dots, \boldsymbol{v_6}]$.

Table 5
Summary of proposed rules for defining imperfections according to DD1.

Imperfection	Description	Illustrations
Sway	• The sway imperfections defined at each storey should act in the same direction and where present, the direction of the sway imperfections should match the direction of the applied lateral loads. • In the absence of lateral loads, both sway directions should be checked and the direction that yields the lowest ultimate capacity should be chosen; for frames that exhibit horizontal symmetry, only one direction needs to be checked.	Pinned supports
Bow	• The bow imperfections of the beams should act downwards. • The bow imperfections of the first storey columns should act in the same direction as the sway imperfection for pinned supports and in the opposite direction for fixed supports. • The direction of the bow imperfections of subsequent columns should alternate starting from the first storey moving upwards.	Fixed supports

4.2.3. EM3

EM3 uses the first sway mode and a selection of non-sway modes as dictated by their eigenvalues under the design loading. Using only the first sway mode allows for sway imperfections to be defined without potentially adverse interference from higher order sway modes, as discussed further in Section 5. The sway imperfections introduced through the first sway mode also typically act all in the same direction, which was a key characteristic observed in the most severe imperfection shapes of the stability-governed frames in the IMC study. For the non-sway modes, the eigenvalue limit provided in [33] for the consideration of second order effects is utilised such that all non-sway modes with $\alpha_{\mathrm{cr,ns}} < 25$ are used to define the imperfection. It should be noted that the $\alpha_{\mathrm{cr,ns}}$ values utilised herein were determined based on eigenvalues at the benchmark ultimate load level α_{u} [40].

4.3. Scaling options

4.3.1. Scaling option A

In scaling option A, A is defined by a set of scale factors denoted A_0. Obtaining A_0 involves first classifying each eigenmode as either a sway mode or non-sway mode, as is described within Section 4.1.2. Once classified, the scale factor for each sway mode and a non-sway mode is taken as the corresponding amplitude limit, as described in Section 2.1.3. The member length, as required for obtaining the scale factor for the non-sway modes, is taken as the length of the member within which the maximum displacement is reached. Note that in scaling option A, since the amplitude limit is applied to each individual eigenmode, the amplitude of the resulting combination of these modes (i.e. the applied imperfection) can exceed, or indeed fall short of, the limit.

4.3.2. Scaling option B

Scaling option B uses a modified set of scale factors initially based on A_0. The intent behind scaling option B is to produce imperfections that are of a similar shape to those of scaling option A, while providing more control over the imperfection amplitude to reduce the extent to which the prescribed limits are violated. The modified scale factors are obtained by defining two auxiliary imperfections formed by splitting the eigenmodes into two groups according to their classification. The two auxiliary imperfections correspond to: (1) a sway-based imperfection

u_0^{sw}, calculated as the sway eigenmodes V^{sw} multiplied by the set of sway scale factors A_0^{sw}, and (2) a non-sway-based imperfection u_0^{ns}, calculated as the non-sway eigenmodes V^{ns} multiplied by the set of non-sway scale factors A_0^{ns}. For each auxiliary imperfection, the corresponding imperfection utilisation vectors U_I^{sw} and U_I^{ns} (see Section 3.1.2), are then calculated and a modified set of sway and non-sway scale factors are obtained as follows:

$$A^{\mathrm{sw}} = \frac{A_0^{\mathrm{sw}}}{\max(U_I^{\mathrm{sw}})} A^{\mathrm{ns}} = \frac{A_0^{\mathrm{ns}}}{\max(U_I^{\mathrm{ns}})} \tag{9}$$

This step ensures that the amplitudes of both auxiliary imperfections under the modified scale factors independently satisfy the prescribed amplitude limits. The full set of modified scale factors A, used to define the imperfections associated with scaling option B, are then obtained by concatenating A^{sw} and A^{ns}.

Alternatively, instead of establishing A and defining the imperfection through $u_0 = VA$, the imperfection can be equivalently obtained by combining the sway-based and non-sway based auxiliary imperfections directly, as follows:

$$u_0 = \frac{u_0^{\mathrm{sw}}}{\max(U_I^{\mathrm{sw}})} + \frac{u_0^{\mathrm{ns}}}{\max(U_I^{\mathrm{ns}})} \tag{10}$$

5. Results and discussion

In this section, the five methods outlined in Section 4 for defining geometric imperfections in planar moment frame systems are examined. Each imperfection definition method is assessed based on its ability to achieve a similar ultimate load to that given by the most severe imperfection shape, as determined in Section 3. The results are summarised in Table 7, where the ultimate loads of each frame for each imperfection definition method α_{d}, normalised against the corresponding benchmark ultimate loads α_{u} (obtained using the most severe imperfection shape—see Fig. 7), are presented. The results from Table 7 are also illustrated graphically in Fig. 8, where the normalised ultimate loads obtained using each imperfection definition method $\alpha_{\mathrm{d}}/\alpha_{\mathrm{u}}$ are overlaid onto the results of the IMC and VAR studies $\alpha_{\mathrm{s}}/\alpha_{\mathrm{u}}$, which are themselves described using boxplots. To aid the explanation of the results, information on the imperfection utilisation for each imperfection definition method, averaged across all frames, is provided in Table 8. Additionally, the normalised ultimate loads for Frames M1 and M2 are plotted against mean(U_I) in Fig. 9, and example imperfections for each imperfection definition method are provided for three frames, Frames M1, M10 and M18, in Figs. 10, 11, and 12, respectively.

From the results, it can be observed that DD1 performs the best of the considered imperfection definition methods, achieving the lowest average normalised ultimate load of 1.009, while maintaining a consistently applied imperfection with an imperfection utilisation of 1.0 throughout. The worst performance of DD1 occurred for Frame M21 with a normalised ultimate load of 1.031. This was due to the frame failing through reaching the CSM strain limit, as opposed to stability (i.e. attainment of the peak load), for which the imperfection shape of DD1 is primarily based. It should be noted that all other imperfection definition methods for which the resulting imperfection was reasonably sized yielded similar normalised ultimate loads for Frame M21.

Imperfection definition method DD2 performs slightly worse than DD1, with a higher average normalised ultimate load of 1.013. The directions of the sway imperfections for DD1 and DD2 were the same due to the similarities between the rules governing the sway imperfections in Table 5 and the rules set out with regards to direction of the first sway mode in Section 4.2; hence, the difference in performance is solely attributed to the influence of the bow imperfections on the beams and columns.

Imperfection definition method EM1 performs well, despite the associated imperfections having a low average mean(U_I) value (i.e.

Table 6
Performance of alternative column imperfection definition strategies during development of DD1. Grey entries indicate which of the two alternating strategies are chosen for each frame according to the proposed set of rules.

Frame	Column imperfection definition strategy				Proposal
M1	1.064	1.064	1.009	1.009	1.009
M2	1.000	1.000	1.021	1.021	1.021
M3	1.013	1.013	1.006	1.006	1.006
M4	1.011	1.011	1.010	1.010	1.010
M5	1.000	1.000	1.039	1.039	1.000
M6	1.000	1.000	1.042	1.042	1.000
M7	1.000	1.000	1.011	1.011	1.000
M8	1.000	1.000	1.015	1.015	1.000
M9	1.045	1.079	1.031	1.016	1.016
M10	1.000	1.010	1.034	1.024	1.024
M11	1.089	1.089	1.010	1.010	1.010
M12	1.021	1.021	1.004	1.004	1.004
M13	1.069	1.069	1.006	1.006	1.006
M14	1.007	1.007	1.014	1.014	1.007
M15	1.051	1.086	1.031	1.011	1.011
M16	1.023	1.016	1.010	1.009	1.009
M17	1.000	1.000	1.003	1.003	1.003
M18	1.021	1.017	1.004	1.008	1.008
M19	1.023	1.023	1.005	1.006	1.006
M20	1.007	1.007	1.009	1.009	1.007
M21	1.032	1.022	1.023	1.031	1.031
Min.	1.000	1.000	1.003	1.003	1.000
Mean	1.023	1.025	1.016	1.014	1.009
Max.	1.089	1.089	1.042	1.042	1.031
CoV	0.025	0.030	0.012	0.011	0.008

mean(U_I) averaged across all frames) of between 0.4 and 0.5 depending upon the chosen scaling option. This is attributed to the rather under-utilised bow imperfections resulting from the fact that the critical eigenmode, for all frames, was a sway mode, which comprised large sway components but small bow components (relative to their respective limits), as highlighted in Table 8 by the disparity between the average mean($U_{I,sw}$) and mean($U_{I,ns}$) values. The large sway imperfections also meant that the sway amplitude limits from storey-to-storey were not always adhered to, as indicated by the average max(U_I) value being greater than 1.0 for scaling option A; this was only the case for the multistorey frames and was resolved in EM1-B, where the rescaling procedure ensured that the limits were met exactly, resulting in a max(U_I) value of 1.0 for each frame. Finally, the adequate performance of EM1, despite the under-utilised bow imperfections, supports the findings of the VAR, where it was concluded that it is most important in moment frames for the sways to be defined correctly.

Imperfection definition methods EM2 and EM3 both introduce additional, typically non-sway, eigenmodes when compared to EM1, resulting in an increase in the average mean($U_{I,ns}$) value and a decrease in the average CoV(U_I) for both scaling options. However, since the additional eigenmodes can either partially negate or compound one another, imperfection amplitudes much larger than intended can result,

as seen for EM2-A and EM3-A. This is illustrated by the average mean (U_I) and max(U_I) values both being much larger than 1.0 and by comparing the size of the imperfections associated with these methods to those of the other methods in Figs. 10, 11, and 12. As a result, while imperfection definition methods EM2-A and EM3-A yield good ultimate capacity predictions on average, the predictions are substantially more scattered than those of DD1 and DD2, with some being overly conservative due to excessively high imperfection amplitudes.

Utilising scaling option B prevents these excessively large imperfections from occurring, as indicated by the average max(U_I) value being close to 1.0, with values of 1.212 and 1.231 for EM2-B and EM3-B, respectively. Unlike with EM1-B, the average max(U_I) values are not exactly 1.0 since multiple modes were combined and these modes were not always entirely pure sway or non-sway as their classification would dictate. In some cases, this results in significant contributions to the sway imperfections from the non-sway modes, which is the reason that, as recommended in Section 4.2, both directions on the first sway mode should be checked when modelling frames without lateral loads. Typically, the direction of the first sway mode that produces sway imperfections in the same direction as the aggregated sway imperfections from the non-sway modes will yield a lower ultimate capacity. It can also be seen that separating the eigenmodes according to their classification

Table 7

Comparison of normalised ultimate loads α_d/α_u associated with each imperfection definition method for all frames. For each method, the ultimate loads are normalised by the corresponding benchmark ultimate load α_u associated with the most severe imperfection shape for each frame.

Frame	DD1	DD2	EM1		EM2		EM3	
			A	B	A	B	A	B
M1	1.009	1.008	1.039	1.039	0.953	1.013	0.922	1.002
M2	1.021	1.010	1.010	1.010	1.016	1.025	1.025	1.027
M3	1.006	1.014	1.011	1.011	1.016	1.013	1.011	1.011
M4	1.010	1.015	1.012	1.012	1.019	1.015	1.012	1.012
M5	1.000	1.023	1.024	1.024	1.018	1.022	1.019	1.022
M6	1.000	1.024	1.017	1.017	1.013	1.016	1.013	1.015
M7	1.000	1.008	1.005	1.005	1.001	1.004	1.001	1.003
M8	1.000	1.005	1.007	1.007	1.013	1.007	0.999	1.004
M9	1.016	1.018	1.018	1.047	0.905	1.059	0.912	1.016
M10	1.024	1.018	1.005	1.018	1.050	1.089	1.043	1.043
M11	1.010	1.000	1.053	1.053	0.960	1.045	0.883	1.041
M12	1.004	1.011	1.016	1.016	1.000	1.012	1.007	1.008
M13	1.006	1.000	1.048	1.048	0.964	1.032	0.896	1.028
M14	1.007	1.010	1.011	1.011	1.012	1.012	1.012	1.012
M15	1.011	1.000	1.017	1.058	0.926	1.072	0.926	1.043
M16	1.009	1.020	1.017	1.019	1.000	1.020	1.013	1.020
M17	1.003	1.004	1.001	1.001	1.014	1.005	1.001	1.001
M18	1.008	1.006	1.006	1.014	0.992	1.013	1.002	1.009
M19	1.006	1.018	0.996	1.009	1.003	1.012	1.001	1.012
M20	1.007	1.002	0.986	1.008	1.006	1.018	0.986	1.008
M21	1.031	1.035	1.024	1.031	0.971	1.030	1.027	1.031
Min.	1.000	1.000	0.986	1.001	0.905	1.004	0.883	1.001
Mean	1.009	1.012	1.015	1.022	0.993	1.025	0.986	1.017
Max.	1.031	1.035	1.053	1.058	1.050	1.089	1.043	1.043
CoV	0.008	0.009	0.015	0.016	0.034	0.022	0.047	0.013
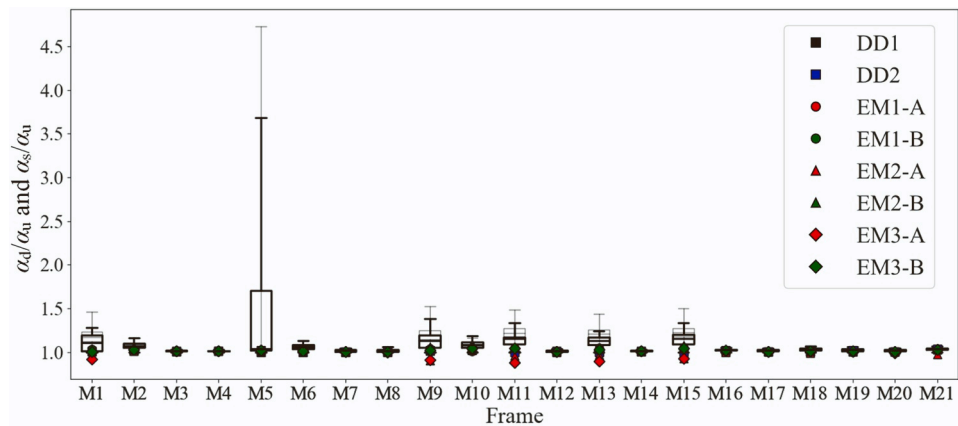
(a) Data presented using full scale on vertical axis
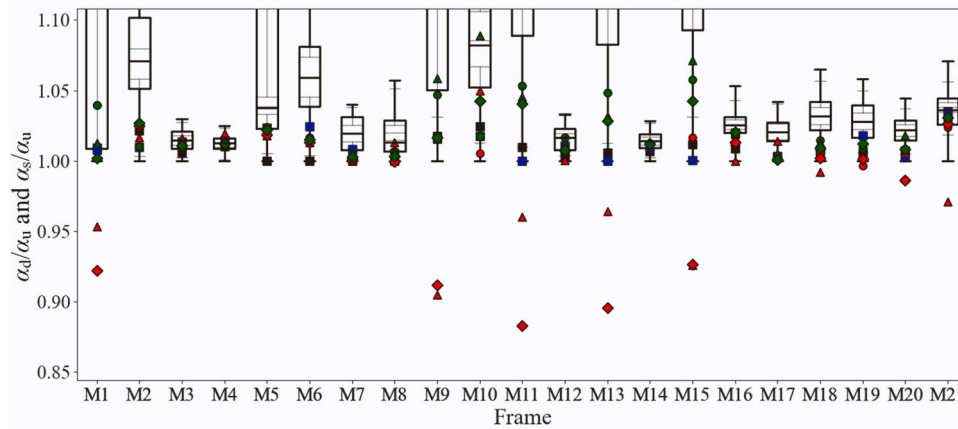
(b) Data presented using focused scale on vertical axis

Fig. 8. Comparison of normalised ultimate loads determined using each imperfection definition method for all frames (α_d/α_u). The thicker and thinner boxplots represent data gathered within the IMC and VAR studies, respectively, with normalised ultimate loads denoted α_s/α_u.

Table 8
Comparison of imperfection utilisation vector for each imperfection definition method.

Average across all frames		DD1	DD2	EM1		EM2		EM3	
				A	B	A	B	A	B
U_{I}	Min.	1.000	1.000	0.056	0.053	0.528	0.255	0.286	0.155
	Mean	1.000	1.000	0.473	0.419	1.526	0.679	1.100	0.625
	Max.	1.000	1.000	1.207	1.000	3.791	1.212	2.371	1.231
	CoV	0.000	0.000	0.992	0.992	0.687	0.554	0.759	0.732
$U_{\text{I,sw}}$	Min.	1.000	1.000	0.800	0.759	1.116	0.810	1.047	0.833
	Mean	1.000	1.000	0.993	0.879	1.606	0.921	1.267	0.962
	Max.	1.000	1.000	1.207	1.000	2.410	1.037	1.525	1.109
	CoV	0.000	0.000	0.187	0.187	0.173	0.174	0.217	0.210
$U_{\text{I,ns}}$	Min.	1.000	1.000	0.056	0.053	0.746	0.259	0.408	0.162
	Mean	1.000	1.000	0.141	0.124	1.488	0.526	0.994	0.408
	Max.	1.000	1.000	0.263	0.206	2.918	0.999	2.080	0.842
	CoV	0.000	0.000	0.512	0.512	0.641	0.591	0.716	0.702
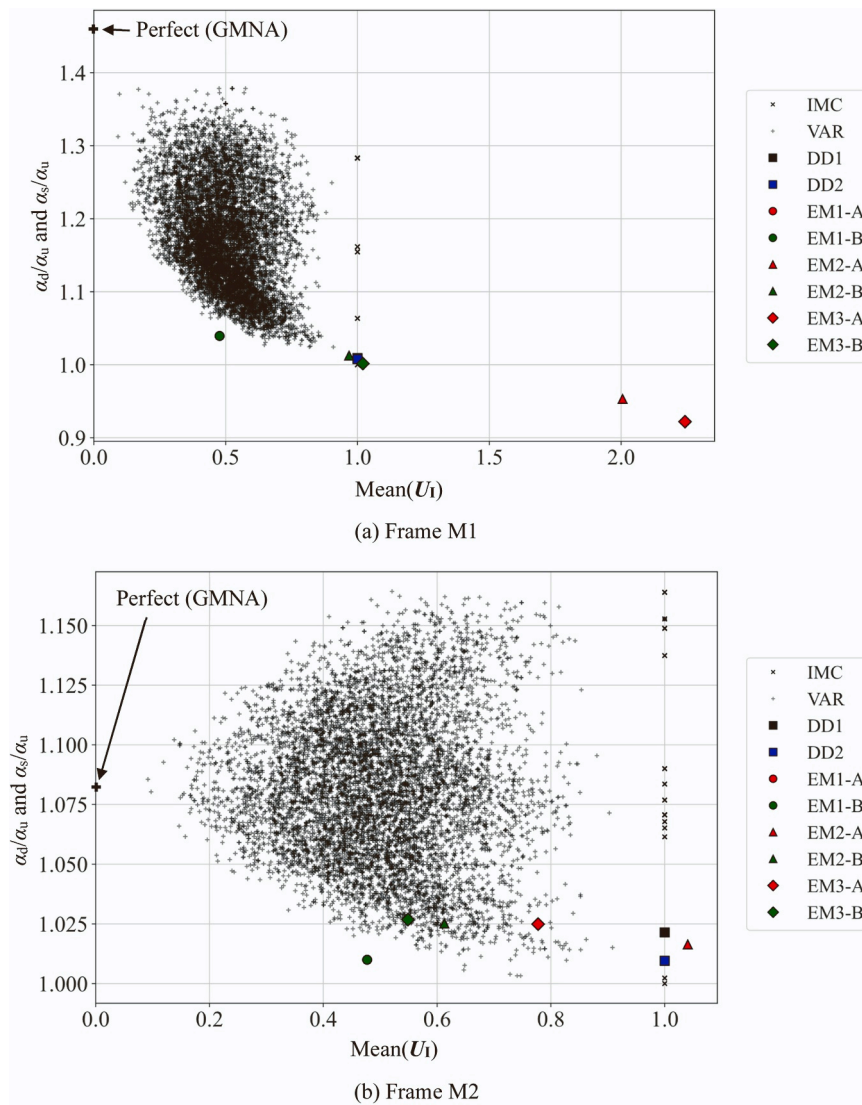
Fig. 9. Normalised ultimate load against mean imperfection utilisation vector for (a) Frame 1 and (b) Frame M2 from the results of the IMC and VAR studies ($\alpha_{\text{s}}/\alpha_{\text{u}}$), and considered imperfection definition methods ($\alpha_{\text{d}}/\alpha_{\text{u}}$).

prior to rescaling led to well-balanced imperfections with similar contributions from both sway and non-sway sources irrespective of the ratio of the number of sway to non-sway eigenmodes being considered, unlike with scaling option A where this ratio usually dictated whether the imperfection was sway or non-sway dominated.

Finally, imperfection definition method EM3 performs slightly better than EM2 due to the omission of higher order sway modes. As alluded to in Section 4.2.3, the sway contributions from higher order sway modes can interfere with the sway contributions from the first sway mode, with these contributions in some cases cancelling out, resulting in almost no
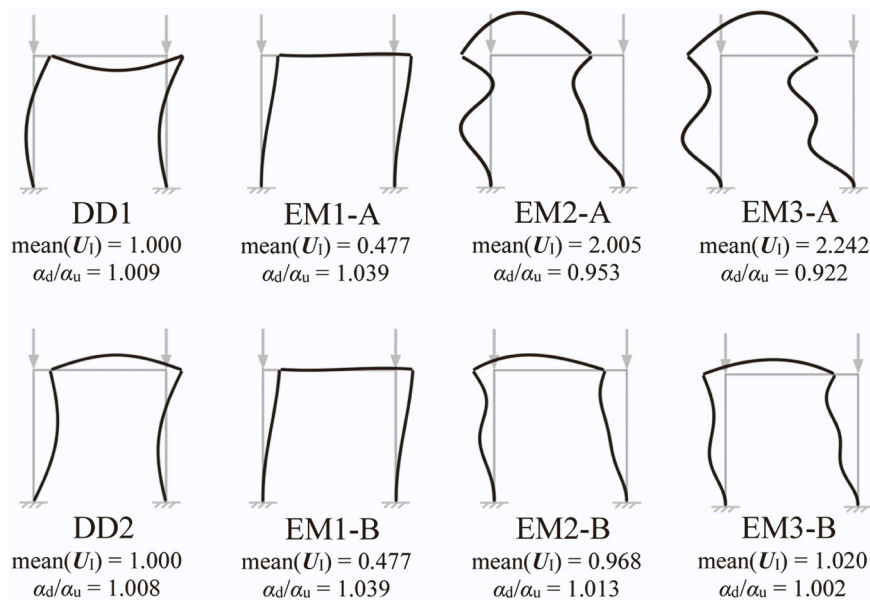
Fig. 10. Frame M1 imperfections corresponding to each of the considered direct definition-based (DDX) and eigenmode-based (EMX-Y) imperfection definition methods, where mean(U_I) is the average of the imperfection utilisation vector and α_d/α_u is the ultimate load normalised against the benchmark ultimate load factor $\alpha_u = 0.690$ associated with the most severe imperfection shape. All imperfections are plotted to the same scale of 50:1.
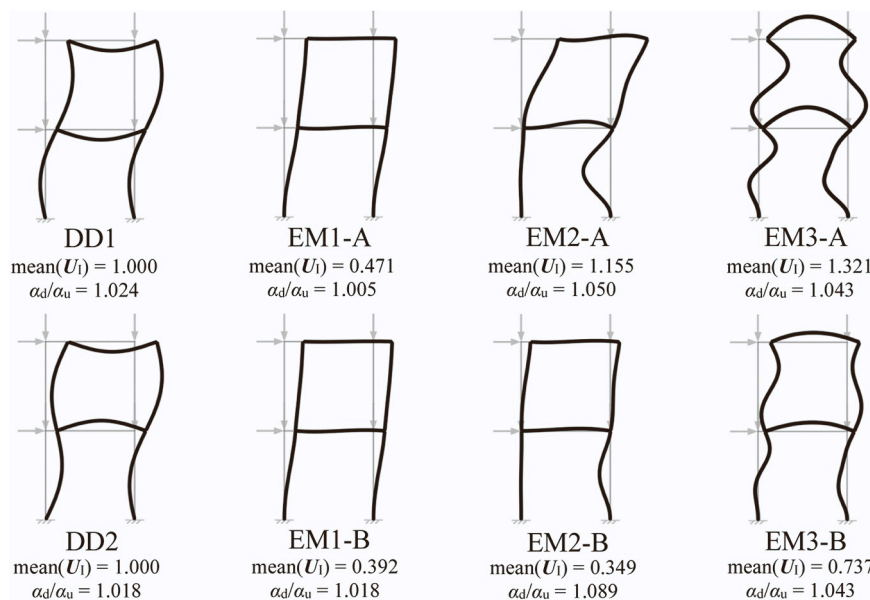

Fig. 11. Frame M10 imperfections corresponding to each of the considered direct definition-based (DDX) and eigenmode-based (EMX-Y) imperfection definition methods, where mean(U_I) is the average of the imperfection utilisation vector and α_d/α_u is the ultimate load normalised against the benchmark ultimate load factor $\alpha_u = 0.614$ associated with the most severe imperfection shape. All imperfections are plotted to the same scale of 50:1.

sway imperfections. This is seen in Fig. 11 for Frame M10 where the sway imperfections on the first storey level are greatly diminished for EM2 for either scaling option, while the sway imperfections remain well-defined for EM3.

Based on the obtained results, the recommended direct definition-based method is DD1 and the recommended eigenmode-based method is EM3-B.

6. Worked examples

In this section, three worked examples are presented to illustrate the application of the two recommended imperfection definition methods, DD1 and EM3-B.

Worked example 1 (WE1) is based upon one of the frames that has already been presented, Frame M15, while worked examples 2 (WE2) and 3 (WE3) introduce two new frame configurations, as shown in Fig. 13, which have been adapted from [41]. Since no IMC study was conducted for Frames WE2 and WE3, the benchmark ultimate load factor used to scale the eigenvalues for EM3-B was established as $\alpha_u = \alpha_{d,DD1}$, where $\alpha_{d,DD1}$ is the ultimate load factor associated with DD1.

The imperfections resulting from the application of DD1 are shown in Fig. 14 for each of the three worked examples. Figs. 15, 16, and 17 provide a breakdown of the process by which the imperfections associated with EM3-B are obtained for worked examples 1, 2, and 3, respectively. Further details specific to each worked example are provided within the following sections.
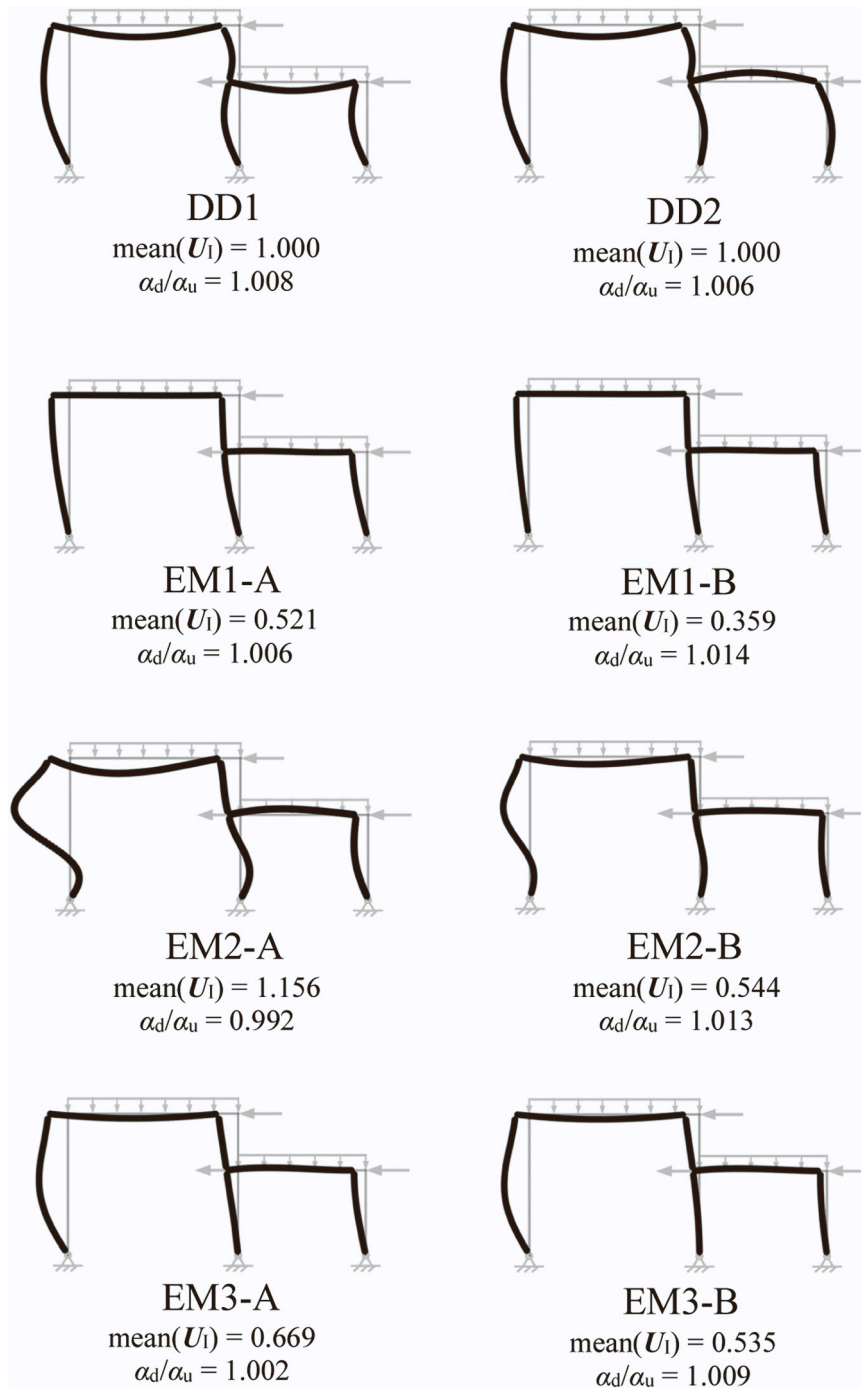
Fig. 12. Frame M18 imperfections corresponding to each of the considered direct definition-based (DDX) and eigenmode-based (EMX-Y) imperfection definition methods, where mean(U_I) is the average of the imperfection utilisation vector and α_d/α_u is the ultimate load normalised against the benchmark ultimate load factor $\alpha_u = 1.051$ associated with the most severe imperfection shape. All imperfections are plotted to the same scale of 50:1.

6.1. Worked example 1

Worked example 1 considers a multistorey frame with fixed supports and subjected to vertical loads only. The height of the frame is 20.0 m, from which $H/400 = 20000/400 = 50.0$ mm. Within each storey, a sway deflection limit of $H_s/400 = 10000/400 = 25.0$ mm applies. Each member is of length $L = 10.0$ m and has an HEB 340 cross-section that, when buckling about its major axis, attracts an imperfection factor of 0.34; hence the imperfection amplitude limit on each bow imperfection is given as $\max(0.34\,L/150,\ L/1000) = 0.00227\,L = 0.00227 \times 10000 = 22.7$ mm.

6.1.1. DD1

The amplitude of the sway imperfections are such that the sways between storeys achieve their limit of 25.0 mm resulting in a 50.0 mm sway deflection at the top of the frame. Since the frame is symmetric, the sway direction can be chosen arbitrarily assuming that the bow imperfections on the first storey columns are defined in the opposite direction due to the fixed boundary conditions. Taking the sway direction to the right, the bow imperfections on the first storey columns lie to the left with the direction then alternating with each subsequent storey. The direction of the bow imperfections in the beams are such that they act downwards. The amplitude of the bow imperfections throughout were
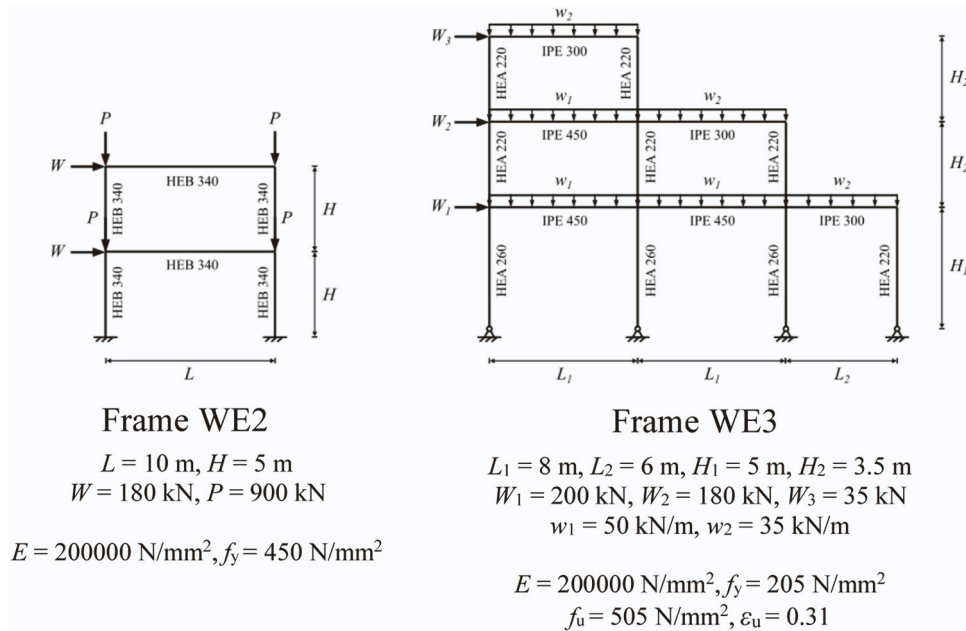
Fig. 13. Two additional frame configurations from [41] to provide worked examples showcasing the imperfection definition methods DD1 and EM3-B.
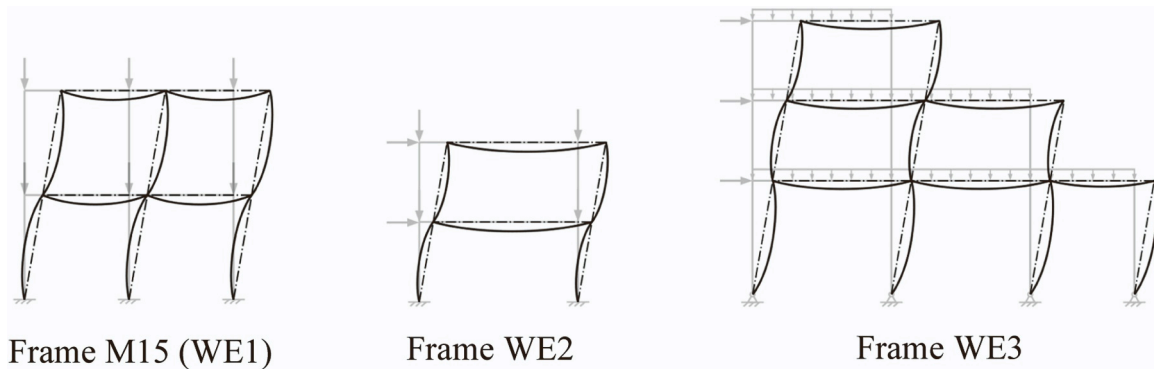

Fig. 14. Imperfections associated with imperfection definition method DD1 for the three worked examples corresponding to Frames M15 (WE1), WE2, and WE3.

equal to the limit of 22.7 mm. This imperfection yielded a normalised ultimate load of $\alpha_d/\alpha_u = 1.011$ (i.e. the imperfection defined using DD1 led to an ultimate load that was very close to that achieved with the most severe imperfection shape).

6.1.2. EM3-B

As per the mode selection criteria of EM3, only the first sway mode i.e. Mode 1 (sw) is used to form the sway-based imperfection; higher order sway modes, such as Mode 2 (sw), are omitted. Based upon the eigenvalues under the design loading, the non-sway-based imperfection consists of Modes 3 (ns) to 16 (ns) with Mode 17 (ns) being the first mode to exceed the limit of 25. Since the frame is without lateral loads, both directions of the first sway mode are considered when establishing the sway-based imperfection; this is done despite the frame being symmetric because of how the sway-based and non-sway-based imperfections can interact with each other. The scale factor on the first sway mode is 50.0 mm with the scale factors on each of the non-sway modes being 22.7 mm. Using the established scale factors, the modes are combined to give two (i.e. positive and negative) sway-based imperfections and a non-sway-based imperfection. The imperfection utilisation of the sway-based and non-sway-based imperfections are then calculated. The maximum imperfection utilisation for both the positive and negative sway-based imperfections is 1.285, corresponding to the

sway deflection at the first storey level. The non-sway-based imperfection utilisation reaches a maximum of 3.342 corresponding to an imperfection of 75.9 mm within the right most first storey column. The two sway-based imperfections and non-sway-based imperfection are subsequently rescaled according to their maximum imperfection utilisation by multiplying by 1/1.285 and 1/3.342, respectively. The two rescaled sway-based imperfections are then independently combined with the rescaled non-sway-based imperfection resulting in two final imperfections for which the ultimate capacities are calculated. The imperfection resulting from the combination of the negative-sway-based imperfection and the non-sway-based imperfection yields the lowest normalised ultimate load of $\alpha_d/\alpha_u = 1.043$; this is therefore chosen as the imperfection to be applied to the frame.

6.2. Worked example 2

Worked example 2 considers another multistorey frame with fixed supports but now with lateral loads. The height of the frame is 10.0 m, thus $H/400 = 10000/400 = 25.0$ mm, and a $H_s/400 = 5000/400 = 12.5$ mm sway deflection limit applies between storeys. All members of the frame have an HEB 340 cross-section, with a yield stress close to that of S460; hence, for major axis buckling, an imperfection factor of 0.21 was used. Therefore, the bow imperfection limits are given
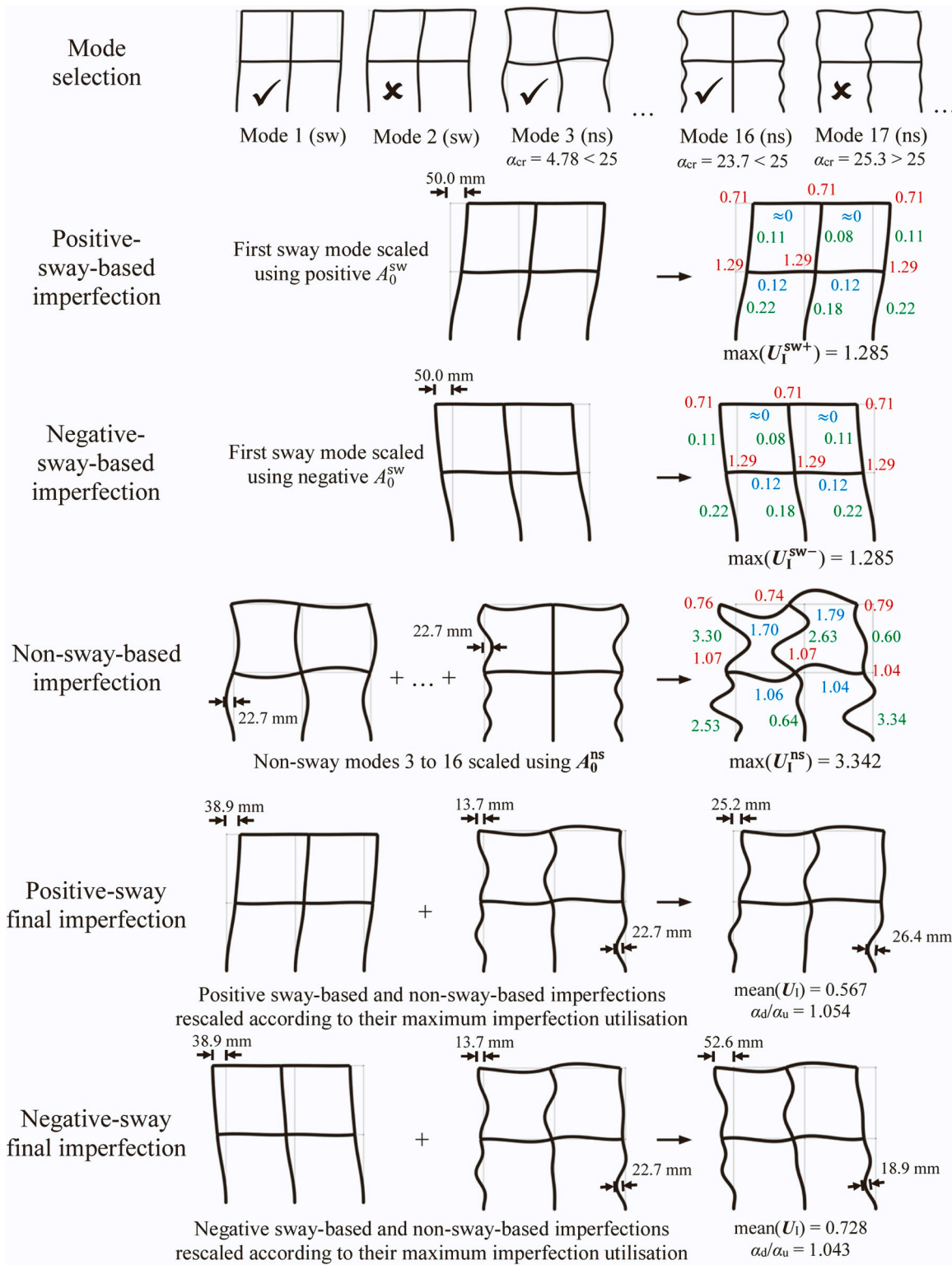
Fig. 15. Worked example 1 – Process of obtaining the imperfection associated with imperfection definition method EM3-B for Frame M15 (WE1).

by $\max(0.21\ L/150, L/1000) = 0.0014\ L$, which produce 14.0 mm and 7.0 mm limits in the beams and columns, respectively.

6.2.1. DD1

The sway direction is dictated by the direction of the lateral loading, hence to the right. Given the fixed boundary conditions, the bow imperfections in the first storey columns are therefore applied in the opposite direction (i.e to the left). The bow imperfections in the beams

act downwards, and the amplitudes of the sway imperfections and bow imperfections are all such that their respective amplitude limits are satisfied.

6.2.2. EM3-B

The mode selection process identifies the first sway mode, Mode 1 (sw), to be used as the sway-based imperfection, and a single non-sway mode, Mode 3 (ns), to be used as the non-sway-based imperfection. The
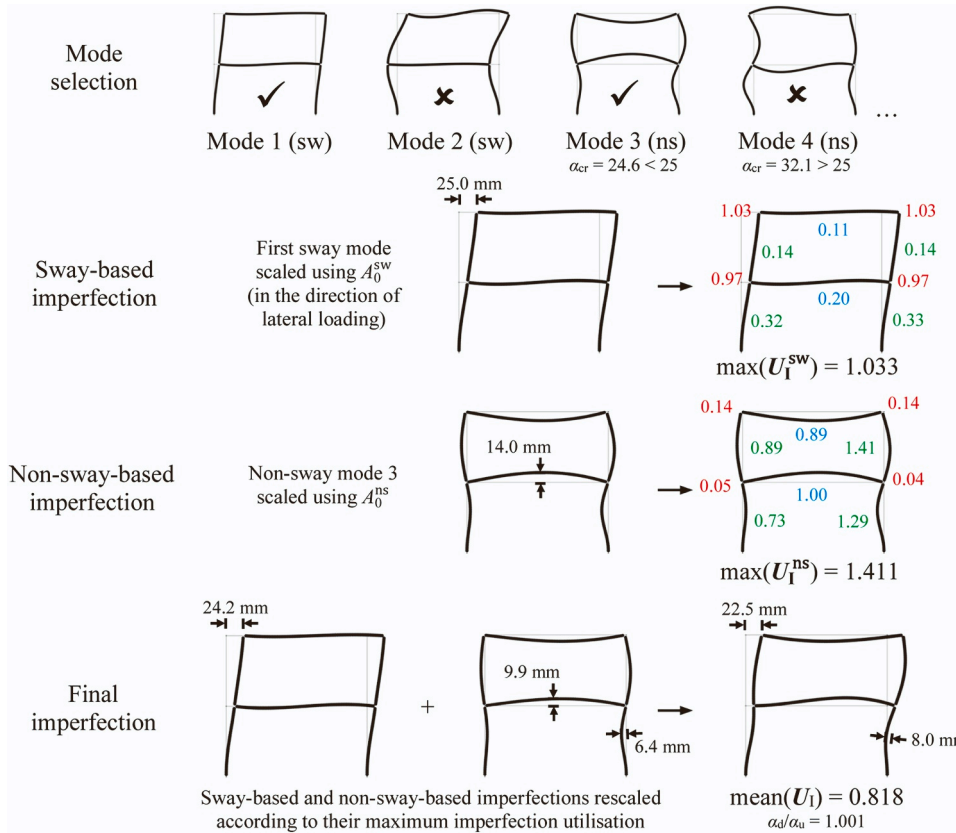
Fig. 16. Worked example 2 – Process of obtaining the imperfection associated with imperfection definition method EM3-B for Frame WE2.
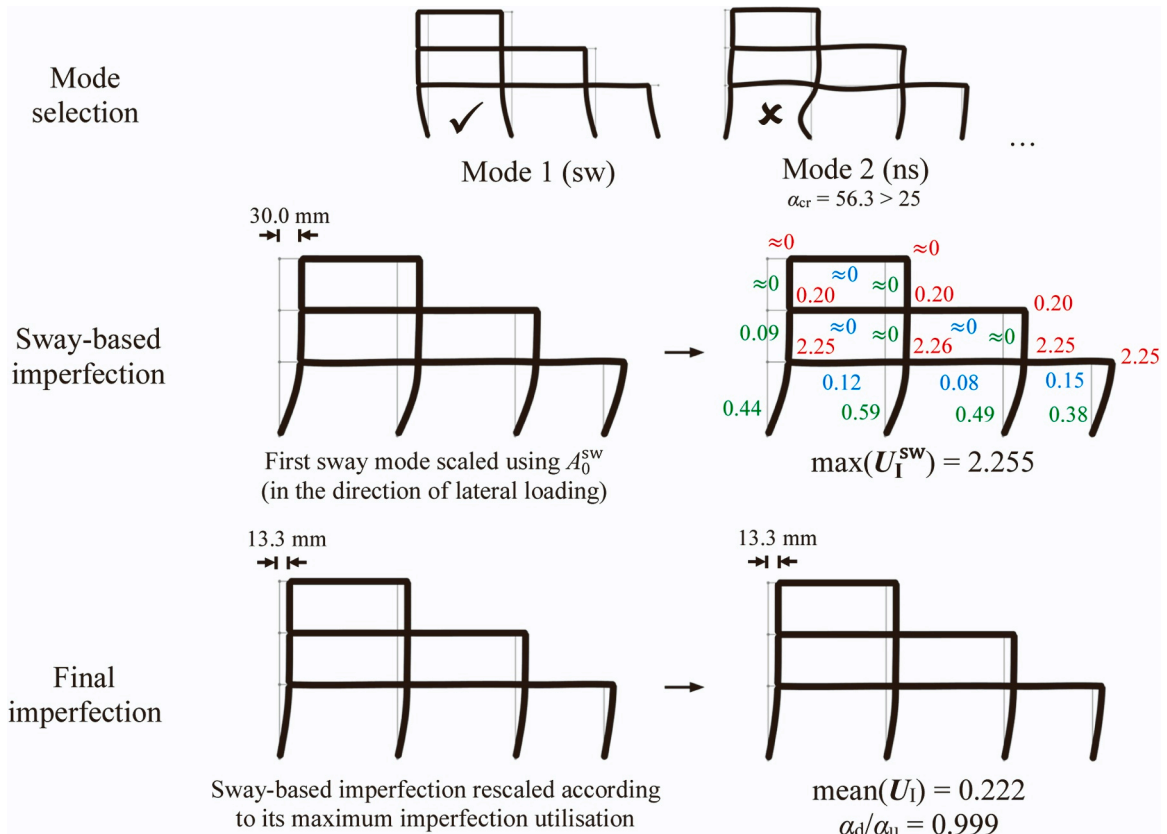

Fig. 17. Worked example 3 – Process of obtaining the imperfection associated with imperfection definition method EM3-B for Frame WE3.

scale factors on modes 1 and 3 are 25.0 mm and 14.0 mm, respectively, the latter corresponding to the bow imperfection limit on the first storey beam, which is where Mode 3 (ns) achieves its maximum displacement. Unlike with worked example 1, the sway direction is established through the direction of the lateral loading, meaning that there is only one sway-based imperfection to consider. The maximum imperfection utilisation of the sway-based and non-sway-based imperfections are calculated as 1.033 and 1.411, respectively. The two imperfections are rescaled according to these maximum imperfection utilisations and combined to give the final imperfection that yields a normalised ultimate load of 1.001 (normalised against $\alpha_{d,DD1}$).

6.3. Worked example 3

Worked example 3 considers an asymmetric frame with pinned supports subjected to vertical and lateral loads. The height of the frame is 12.0 m, thus $H/400 = 12000/400 = 30.0$ mm, and a $H_s/400 = 5000/400 = 12.5$ mm sway deflection limit applies between the foundation and the first storey, with a $3500/400 = 8.8$ mm storey sway deflection limit applying from there upwards. The frame is composed of members with differing lengths and cross-sections for which the bow imperfection limits range from 7.9 to 11.3 mm.

6.3.1. DD1

The lateral loads dictate that the sways should act to the right. In contrast with worked examples 1 and 2, the pinned supports dictate that the bow imperfections in the first storey columns should act in the same direction, also to the right. As before, the directions of the bow imperfections in the remaining columns alternate going upwards and the bow imperfections in the beams act downwards. The amplitudes of the sway imperfections and bow imperfections are all such that their respective amplitude limits are satisfied.

6.3.2. EM3-B

Mode 1 (*sw*), the first sway mode, is chosen to define the sway-based imperfection. From the eigenvalues under the design loading, no non-sway modes satisfy the selection criteria (i.e. $\alpha_{cr,ns} < 25$); hence, there is no non-sway-based imperfection. The scale factor on the first sway mode is 30.0 mm with the direction being dictated by the lateral loads. The maximum imperfection utilisation is located at the first storey level since most of the sway deflection in Mode 1 (*sw*) ($2.255 \times 12.5 = 28.2$ mm of the 30.0 mm in total) occurs between the foundation and the first storey. Once rescaled, the final imperfection achieves an imperfection utilisation of 1.0 within the first storey level, corresponding to a sway imperfection of 12.5 mm between the foundation and the first storey, and with an overall sway imperfection of $30.0/2.255 = 13.3$ mm at the top of the frame. The normalised ultimate load for this imperfection is 0.999 (normalised against $\alpha_{d,DD1}$).

7. Conclusions

Practical recommendations for the safe and accurate definition of geometric imperfections in planar moment frames for design by advanced analysis (GMNIA and GNIA) have been proposed herein. Two types of imperfection definition method were considered depending upon whether the imperfection was: (1) defined directly or (2) established through the scaling of eigenmodes. In total, five methods were defined, two direct definition-based methods and three eigenmode-based methods, with variations on each of the eigenmode-based methods depending upon the approach to scaling. The methods were evaluated against 'worst-case' benchmark results obtained from an imperfection combination study that exhaustively revealed the most severe imperfection shape. Based on the results, a recommended strategy for each approach to introducing imperfections (i.e. direct definition and the scaling of eigenmodes) has been developed. The recommended direct definition-based method introduces a sway imperfection in

sympathy with the applied lateral loading and member imperfections with alternating directions between storeys, as dictated by the column base boundary conditions. The recommended eigenmode-based method uses the first sway mode and all non-sway modes for which $\alpha_{cr,ns} < 25$, where $\alpha_{cr,ns}$ is the eigenvalue under the design loading. A scaling approach (scaling option B) is proposed as a means of combining several eigenmodes, while producing appropriately sized and proportioned imperfections. Overall, the two recommended imperfection definition methods (DD1 and EM3-B) provide accurate and consistent capacity predictions compared with the benchmark results. Work is ongoing to extend the design provisions to braced frames and three-dimensional systems.

CRediT authorship contribution statement

M. Ahmer Wadee: Conceptualization, Methodology, Resources, Supervision, Writing – review & editing. **Leroy Gardner:** Conceptualization, Investigation, Methodology, Resources, Supervision, Writing – review & editing. **Harry Slack:** Data curation, Formal analysis, Investigation, Writing – original draft, Conceptualization, Methodology, Validation. **Fiona Walport:** Data curation, Investigation, Methodology, Writing – original draft, Writing – review & editing. **Hou Un Chan:** Data curation, Formal analysis, Investigation, Validation, Writing – original draft.

Declaration of Competing Interest

The authors declare that they have no known competing financial interests or personal relationships that could have appeared to influence the work reported in this paper.

Acknowledgements

References

[1] Fieber A, Gardner L, Macorini L. Design of structural steel members by advanced inelastic analysis with strain limits. Eng Struct 2019;199:109624. https://doi.org/10.1016/j.engstruct.2019.109624.
[2] Liew JYR, Chen WF, Chen H. Advanced inelastic analysis of frame structures. J Constr Steel Res 2000;55:245–65. https://doi.org/10.1016/S0143-974X(99)00088-7.
[3] Buonopane SG, Schafer BW. Reliability of steel frames designed with advanced analysis. J Struct Eng ASCE 2006;132:267–76. https://doi.org/10.1061/(asce)0733-9445(2006)132:2(267).
[4] Chan SL, Chen WF. Advanced analysis as a new dimension for structural steel design. Adv Steel Constr 2005;1:87–102.
[5] Trahair NS, Chan SL. Out-of-plane advanced analysis of steel structures. Eng Struct 2003;25:1627–37. https://doi.org/10.1016/S0141-0296(03)00134-2.
[6] Walport F, Chan HU, Gardner L, Nethercot DA. Design of stainless steel structural systems by GMNIA with CSM strain limits. Eng Struct 2023;276:115339. https://doi.org/10.1016/j.engstruct.2022.115339.
[7] Fieber A, Gardner L, Macorini L. Structural steel design using second-order inelastic analysis with strain limits. J Constr Steel Res 2020;168:105980. https://doi.org/10.1016/j.jcsr.2020.105980.
[8] Gardner L, Yun X, Fieber A, Macorini L. Steel design by advanced analysis: material modeling and strain limits. Engineering 2019;5:243–9. https://doi.org/10.1016/j.eng.2018.11.026.
[9] AISC 360–16, AISC 360 – Specification for structural steel buildings, American Institute of Steel Construction (2016).
[10] AISC 370–21, AISC 370 – Specification for structural stainless steel buildings, American Institute of Steel Construction (2021).
[11] prEN 1993–1-14, EN 1993-1-14 – Eurocode 3: Design of steel structures – Part 1–14: Design assisted by finite element analysis, (2023) CEN Enquiry.
[12] Müller A, Vild M, Taras A. Decision tree for local + global imperfection combinations in double-symmetric prismatic members – Practical

recommendations in the framework of advanced analysis. Steel Constr 2023;16: 2–15. https://doi.org/10.1002/stco.202200041.

[13] Chan HU, Walport F, Gardner L. Equivalent sway imperfections and sway-member imperfection combinations for GMNIA-based steel design. Structures 2024;62: 106216. https://doi.org/10.1016/j.istruc.2024.106216.

[14] ABAQUS. SIMULIA-Dassault Systémes: Analysis User's Guide. Providence, USA, USA: Dassault Systémes Simulia Corp; 2021.

[15] Walport F, Gardner L, Nethercot DA. A method for the treatment of second order effects in plastically-designed steel frames. Eng Struct 2019;200:109516. https://doi.org/10.1016/j.engstruct.2019.109516.

[16] Ziemian CW, Ziemian RD. Steel benchmark frames for structural analysis and validation studies: finite element models and numerical simulation data. Data Brief 2021;39:107564. https://doi.org/10.1016/j.dib.2021.107564.

[17] Fieber A, Gardner L, Macorini L. Formulae for determining elastic local buckling half-wavelengths of structural steel cross-sections. J Constr Steel Res 2019;159: 493–506. https://doi.org/10.1016/j.jcsr.2019.04.037.

[18] Yun X, Gardner L. Stress-strain curves for hot-rolled steels. J Constr Steel Res 2017; 133:36–46. https://doi.org/10.1016/j.jcsr.2017.01.024.

[19] Gardner L, Yun X. Description of stress-strain curves for cold-formed steels. Constr Build Mater 2018;189:527–38. https://doi.org/10.1016/j.conbuildmat.2018.08.195.

[20] Walport F, Gardner L, Nethercot DA. Design of structural stainless steel members by second order inelastic analysis with CSM strain limits. Thin-Walled Struct 2021; 159:107267. https://doi.org/10.1016/j.tws.2020.107267.

[21] Gardner L, Yun X, Walport F. The continuous strength method - review and outlook. Eng Struct 2023;275:114924. https://doi.org/10.1016/j.engstruct.2022.114924.

[22] Liew A, Gardner L. Ultimate capacity of structural steel cross-sections under compression, bending and combined loading. Structures 2015;1:2–11. https://doi.org/10.1016/j.istruc.2014.07.001.

[23] Yun X, Gardner L, Boissonnade N. The continuous strength method for the design of hot-rolled steel cross-sections. Eng Struct 2018;157:179–91. https://doi.org/10.1016/j.engstruct.2017.12.009.

[24] Gardner L, Fieber A, Macorini L. Formulae for calculating elastic local buckling stresses of full structural cross-sections. Structures 2019;17:2–20. https://doi.org/10.1016/j.istruc.2019.01.012.

[25] Quan C, Kucukler M, Gardner L. Out-of-plane stability design of steel beams by second-order inelastic analysis with strain limits. Thin-Walled Struct 2021;169: 108352. https://doi.org/10.1016/j.tws.2021.108352.

[26] Wakabayashi M, Matsui C, Minami K, Mitani I. Inelastic behavior of full-scale steel frames with and without bracings. Bull Disaster Prev Res Inst 1974;24:1–23.

[27] Wakabayashi M, Matsui C. Experimental studies on the elastic plastic stability of steel frames - Part 2: Portal frames composed of H-shape members. Trans Archit Inst Jpn 1972;193:17–27.

[28] M. Kucukler, Stiffness Reduction Approach for Structural Steel Design, Imperial College London, 2015.

[29] ECCS, Ultimate limit state calculations of sway frames with rigid joints, No. 33, Technical Committee 8 of the European Convention for Constructional Steelwork (ECCS) 1984 (1984).

[30] EN 1090–2, EN 1090–2 - Execution of steel structures and aluminium structures. Part 2: Technical requirements for steel structures., BSI, 2018.

[31] Basaglia C, Camotim D, Silvestre N. Torsion warping transmission at thin-walled frame joints: Kinematics, modelling and structural response. J Constr Steel Res 2012;69:39–53. https://doi.org/10.1016/j.jcsr.2011.07.016.

[32] Van Rossum G, Drake FL. Python 3 Reference Manual. Scotts Valley, CA: CreateSpace; 2009.

[33] EN 1993–1-1, Eurocode 3 – Design of steel structures – Part 1–1: General rules and rules for buildings, CEN (2022).

[34] Walport F, Gardner L, Nethercot DA. Equivalent bow imperfections for use in design by second order inelastic analysis. Structures 2020;26:670–85. https://doi.org/10.1016/j.istruc.2020.03.065.

[35] Sobol IM. On the distribution of points in a cube and the approximate evaluation of integrals. USSR Comput Math Math Phys 1967;7:86–112. https://doi.org/10.1016/0041-5553(67)90144-9.

[36] Jansen MJW. Analysis of variance designs for model output. Comput Phys Commun 1999;117:35–43. https://doi.org/10.1016/S0010-4655(98)00154-4.

[37] Saltelli A, Annoni P, Azzini I, Campolongo F, Ratto M, Tarantola S. Variance based sensitivity analysis of model output. Design and estimator for the total sensitivity index. Comput Phys Commun 2010;181:259–70. https://doi.org/10.1016/j.cpc.2009.09.018.

[38] Shayan S, Rasmussen KJR, Zhang H. On the modelling of initial geometric imperfections of steel frames in advanced analysis. J Constr Steel Res 2014;98: 167–77. https://doi.org/10.1016/j.jcsr.2014.02.016.

[39] Arrayago I, Rasmussen KJR. Influence of the imperfection direction on the ultimate response of steel frames in advanced analysis. J Constr Steel Res 2022;190:107137. https://doi.org/10.1016/j.jcsr.2022.107137.

[40] Walport F, Gardner L, Real E, Arrayago I, Nethercot DA. Effects of material nonlinearity on the global analysis and stability of stainless steel frames. J Constr Steel Res 2019;152:173–82. https://doi.org/10.1016/j.jcsr.2018.04.019.

[41] Walport F, Kucukler M, Gardner L. Stability design of stainless steel structures. J Struct Eng 2022;148:4021225. https://doi.org/10.1061/(ASCE)ST.1943-541X.0003165.